STUDIES OF SILVER (AG) PLASMONICS STRUCTURES INTEGRATED IN SIDE POLISHED OPTICAL FIBER SENSOR

SITI FATIMAH AZ ZAHRA BINTI YUSOFF

INSTITUTE OF GRADUATE STUDIES
UNIVERSITY OF MALAYA
KUALA LUMPUR

2018

STUDIES OF SILVER (AG) PLASMONICS STRUCTURES INTEGRATED IN SIDE POLISHED OPTICAL FIBER SENSOR

SITI FATIMAH AZ ZAHRA BINTI YUSOFF

DISSERTATION SUBMITTED IN FULFILMENT OF THE REQUIREMENTS FOR THE DEGREE OF MASTER OF PHILOSOPHY

INSTITUTE OF GRADUATE STUDIES
UNIVERSITY OF MALAYA
KUALA LUMPUR

2018

UNIVERSITY OF MALAYA
ORIGINAL LITERARY WORK DECLARATION

Name of Candidate: **Siti Fatimah Az Zahra binti Yusoff**

Matric No: **HGG150006**

Name of Degree: **Master of Philosophy**

Title of Project Paper/Research Report/Dissertation/Thesis ("this Work"):

Studies of Silver (Ag) Plasmonics Structures Integrated In Side Polished Optical Fiber Sensor

Field of Study: **Photonics Sciences**

I do solemnly and sincerely declare that:

(1) I am the sole author/writer of this Work;
(2) This Work is original;
(3) Any use of any work in which copyright exists was done by way of fair dealing and for permitted purposes and any excerpt or extract from, or reference to or reproduction of any copyright work has been disclosed expressly and sufficiently and the title of the Work and its authorship have been acknowledged in this Work;
(4) I do not have any actual knowledge nor do I ought reasonably to know that the making of this work constitutes an infringement of any copyright work;
(5) I hereby assign all and every rights in the copyright to this Work to the University of Malaya ("UM"), who henceforth shall be owner of the copyright in this Work and that any reproduction or use in any form or by any means whatsoever is prohibited without the written consent of UM having been first had and obtained;
(6) I am fully aware that if in the course of making this Work I have infringed any copyright whether intentionally or otherwise, I may be subject to legal action or any other action as may be determined by UM.

Candidate's Signature Date:

Subscribed and solemnly declared before,

Witness's Signature Date:

Name:

Designation:

STUDIES OF SILVER (AG) PLASMONICS STRUCTURES INTEGRATED IN SIDE POLISHED OPTICAL FIBER SENSOR

ABSTRACT

Many researchers have a great interest in nanotechnology field specifically in integrating plasmonics nanoparticles (NPs) as a device due to the unique characteristics owned by this noble metallic structure. Surface plasmon resonance (SPR) is the behavior of plasmonics which involves the study on the excitation of surface plasmon polaritons (SPP) at the metal-dielectric interface when interacting with light. In this work, the studies were focused on four main objectives, which are first; to study the effects of silver (Ag) structures with arbitrary shapes at random position, and secondly, is to study the effects of silver nanoparticles (AgNPs) with varying thickness of Ag films. Third objective is to design and fabricate side-polished optical fiber with the performance of AgNPs and lastly to study the application of Ag and the effects of TiO_2 coated on the active area of the optical fiber as a humidity sensor. To accomplish the first objective, an arbitrary shape of Ag structures has been constructed experimentally using electrochemical deposition technique and the optical properties of the structures have been observed using Computer Simulation Technology (CST) Microwave Studio software. The shapes of Ag formed are flower-like structures with distinct petals looks. From the simulation, it has been proven that Ag flower-like structures show an obvious increment in an electromagnetic field due to the hotspots. Effect on varying thickness of AgNPs thin films has been further investigated. The Ag films were fabricated using electron beam (e-beam) evaporation techniques with four different thicknesses. The optical properties of the AgNPs has been observed using CST Microwave Studio software. Another layer of metal oxides, namely titanium oxide (TiO_2) is introduced as another layer, covering the metallic layer in order to study the effect of metal oxides towards the improvement in detection. An optical fiber sensor has been fabricated using side polish unclad single mode fiber (SMF), with Ag and

TiO_2 coating. The main parameters are involved is to improve the quality of the sensor from sensitivity and accuracy point of view. With a right value of metallic layer and the polishing depth of the fiber, the quality of the sensor can be manipulated and optimized for a better application. The sensor with 7 nm Ag and TiO_2 coating shows a better response as the percentage of relative humidity (% RH) increase.

Keywords: silver, plasmonics, nanostructures, side polished optical fiber.

KAJIAN TERHADAP STRUKTUR PLASMONIK PERAK (AG) BERSEPADU DALAM SENSOR GENTIAN OPTIKAL SATU SISI GILAPAN

ABSTRAK

Ramai penyelidik mempunyai minat yang besar dalam bidang nanoteknologi khususnya dalam mengintegrasikan zarah nano plasmonik (NP) sebagai alat kerana ciri-ciri unik yang dimiliki oleh struktur metalik ini. Permukaan resonan plasmon (SPR) adalah tingkah laku plasmonik yang melibatkan kajian pengujaan polarit plasmon permukaan (SPP) pada permukaan logam-dielektrik apabila berinteraksi dengan cahaya. Kajian ini memberi tumpuan kepada empat objektif utama, yang pertama, untuk mengkaji kesan struktur Ag dengan bentuk rawak, dan kedua, untuk mengkaji kesan-kesan zarah nano Ag (AgNPs) dengan ketebalan filem Ag. Objektif ketiga adalah untuk merekabentuk gentian optik yang digilap sisinya dengan prestasi zarah nano Ag dan matlamat terakhir adalah untuk mengkaji aplikasi Ag dan kesan TiO_2 yang bersalut pada kawasan aktif gentian optik sebagai sensor kelembapan. Untuk mencapai objektif pertama, bentuk arbitrase struktur Ag telah dibina secara eksperimen menggunakan teknik pemendapan elektrokimia dan sifat optik struktur telah dikaji menggunakan perisian CST Microwave Studio. Bentuk-bentuk struktur Ag yang telah dibina adalah struktur seperti bunga dengan kelopak yang berbeza kelihatan. Dari simulasi, telah terbukti bahawa struktur bunga Ag menunjukkan kenaikan jelas dalam medan elektromagnetik yang disebabkan oleh titik panas. Kesan kepada ketebalan filem-filem tipis zarah nano Ag telah disiasat selanjutnya. Filem Ag disadur dengan menggunakan teknik penyejatan elektron (e-beam) dengan empat ketebalan yang berlainan. Sifat optik nanopartikel Ag telah diperhatikan dengan menggunakan perisian CST Microwave Studio. Satu lagi lapisan oksida logam, iaitu titanium oksida (TiO_2) diperkenalkan sebagai lapisan lain, meliputi lapisan metalik untuk mengkaji kesan logam oksida ke arah peningkatan pengesanan. Sensor gentian optik telah dibuat menggunakan gentian mod tunggal fiber (SMF), dengan lapisan Ag dan TiO_2.

Parameter utama yang terlibat adalah untuk meningkatkan kualiti sensor dari sudut kepekaan dan ketepatan pandangan. Dengan nilai yang tepat lapisan metalik dan kedalaman kawasan gilapan gentian optik, kualiti sensor dapat dimanipulasi dan dioptimumkan untuk aplikasi yang lebih baik. Sensor dengan lapisan 7 nm Ag dan TiO_2 menunjukkan tindak balas yang lebih baik kerana peratusan kelembapan relatif (% RH) meningkat.

Kata kunci: perak, plasmonik, struktur nano, gentian optik gilapan sisi.

ACKNOWLEDGEMENTS

Alhamdulillah, all praises be to Allah, the almighty God who has given me the strength to keep myself going through and completed this work. For me, to bring this work to an end required a lot of supervision and help from many people and I am grateful to have them along the journey of my research.

I feel fortunate and grateful to have support from my supervisor Prof. Dr. Harith Ahmad as he always helped me and make sure that I can completed my research work smoothly. Also, I would like to give a special appreciation to my other supervisor, Dr. Rozalina Zakaria, for putting her trust on me and give me the opportunity to do this project under her supervision. She gives endless support and guidance that I need so that I can devote myself on completing this research.

Not forgetting, thank you to my lab mates, Kak Syifa, Mezher, and Ainaa who always helped me whenever I need them in terms of research work and moral support. I would also like to thank my colleague at the center, Aisyah, Hazirah, Anir, Nabila, Ezzaty, Farhana, Adawiyah, and Syahirah for their endless support in completing my research and thesis.

My last appreciation goes to my beautiful family especially my parents, Yusoff Ja'afar Sidek and Sahimi Mohamed, who always gives support and encourage me to do this research passionately. Also, I would like to thank my siblings as they always support me without fail.

TABLE OF CONTENTS

LIST OF FIGURES

LIST OF TABLES

LIST OF SYMBOLS AND ABBREVIATIONS

AgNPs	:	Silver Nanoparticles
SPR	:	Surface Plasmon Resonance
LSPR	:	Localized Surface Plasmon Resonance
TiO_2	:	Titanium Oxide
CST	:	Computer Simulation Technology
E-beam	:	Electron beam
SMF	:	Single Mode Fiber
$[Ag (NH_3)_2] OH$	:	Silver Ammonia
AgCl	:	Silver Chloride
E-field	:	Electric field

CHAPTER 1: INTRODUCTION

1.1 Introduction to Plasmonics

Plasmonics is the most interesting topic in nanophotonics field. It is study of confinement of light at nanoscale region which smaller than the scale of light wavelength in free space. The basic study of plasmonics is the interaction process between electromagnetic (EM) fields with the conductive electrons at the metallic surfaces. The confinement of plasmonics in nanoparticles contribute to an enhancement in optical near-field of sub-wavelength dimensions. The utilization of resonance effect to manipulate interactions between light and matter in a sub-wavelength scale is a motivation.

Plasmon can be in many forms, starts from surface plasmon polaritons that propagating along the metal dielectric surfaces to localized surface plasmons as oscillation of electron happened inside metal nanoparticles. This totally depends on the geometry of metal nanostructures and their surrounding environment (Freise, 2012). Researchers tend to reveal great potential of plasmonics study for various applications such as in biological field, photo thermal imaging and therapy (Boken, Khurana, Thatai, Kumar, & Prasad, 2017), optical signal processing (Li, Hong, & Sun, 2011), sub wavelength microscopy (Kroo, Szentirmay, & Walther, 2005) and many more. Since plasmonics have wide range of potential application from electronic to biological field, many methods have been proposed for the synthesis of metal nanoparticles such as electrochemical deposition (Zakaria, Yusoff, Law, Lim, & Ahmad, 2017), vapor deposition (S. Xu et al., 2015), electron beam deposition (Hamdan, Abdullah, Sulaiman, & Zakaria, 2014) and reduction of metal salts with the presence of stabilizers (Boken et al., 2017).

1.2 Motivation of the Study

It is known that factors are affecting spectral position of plasmonics resonance are size and shape of nanoparticles, dielectric of surrounding environment and as well as separation distance between particles (Caucheteur, Guo, & Albert, 2015). The variation of these factors can be tuned based on the individual needs has led to numerous applications. Thus, the urge to study the tunability of plasmonics nanostructures has been raised and the motivation for the application in many fields has been encouraged.

In this study, different shapes of nanostructures was tuned in order to see the performance of plasmonics behavior showed by the nanostructure since different shapes will scatter and absorb light in different way. Also, the interesting way to fabricate nanostructures with arbitrary shapes has urged the researchers to do more research on this factor. Apart from that, the tunability of nanoparticle's size is one of the important factor as optimum size of nanoparticles will give a great enhancement in the plasmonics characteristics. The material used to study the plasmonics characteristic also need to be considered because it is important to have a material which shows strong plasmonics effects with low loss and have a high field enhancement. And lastly, the great advantages showed by optical fiber has been a motivation in the fabrication process of humidity sensor since the optical fiber itself shows a good response, small in size and have a good performance in harsh environment (Urrutia, Goicoechea, & Arregui, 2015). The combination of plasmonics and confinement of light in optical fiber could be a great alternative to increase the performance of the humidity sensor.

1.3 Objectives of the Study

The objectives of this research are identified in order to achieve the aims of the project;

1. To investigate the effect of arbitrary shapes of silver (Ag) structures.
2. To investigate the effect of size of Ag by varying thickness of Ag layer.
3. To design and fabricate plasmonics side polished optical fiber which can be utilized as humidity sensor.
4. To compare the experimental results of humidity sensor between bare optical fiber, Ag and Ag/TiO_2 coated on side polished fiber.

1.4 Thesis Framework

This thesis comprised of three parts, as part A is the comprehensive study on the effects of having different shapes of silver plasmonics structures. Part B discussed on the effects of having different thickness of silver thin layers and the last part is the experimental study on humidity sensor using side polished optical fiber. Simulation studies and experimental results were investigated to see the behavior of having different structures and sizes of metallic particles. The first chapter provides a brief introduction of plasmonics theory, research objectives along with the flow of this research study.

Chapter two gives details to description on the background of research scope, including theoretical models in plasmonics, surface plasmon (SP), surface plasmon resonance (SPR) and localized surface plasmon resonance (LSPR). Brief explanation on metallic nanoparticles and plasmonics optical fiber sensor also will be include in this chapter together with the role of titanium oxide (TiO_2).

The third chapter describes the methodology for the optical characterization of Ag structure on glass substrates. The details on the fabrication process of side polished optical fiber will also discussed in this chapter. The simulation studies for both parts (A and B) will be further explaining using CST Microwave Studio simulation.

The next chapter report on the simulation study and the experimental results of the optical characterization of Ag structures on a glass substrate. Part A discussed on the effect of Ag structures with arbitrary shapes and for part B, we will explore on the effect of having different thicknesses of Ag thin layers. Part C discussed the experimental analysis of Ag and TiO_2 coated on side polished optical fiber. This fabrication will be tested as humidity sensor which will be explained furthermore in this chapter.

Finally, conclusions of this research will be summarized in chapter five including future work.

CHAPTER 2: LITERATURE REVIEW

2.1 Introduction to Plasmonics

2.1.1 Theoretical Models in Plasmonics

In plasmonics study, there are few theoretical models are considered in order to study the surface plasmons and their dispersion relation. An introduction on the theoretical models such as Mie and Drude's models will be explained concisely due to their significant in the plasmonics field.

2.1.1.1 Mie's Theory

Application based on Mie's theory has become broader and has been an interest to the researchers in plasmonics study. This theory was discovered by Gustav Mie in 1908, discussing the computation of light scattering by spherical nanoparticles using Maxwell's electromagnetic theory and explanation on changes in color of metallic particles, which was interpreted as surface plasmon resonance (SPR) later on (Mie, 1908). Solving Maxwell's equation gives results in a relationship of extinction cross section for metallic nanoparticles;

$$\sigma_{ext} = \sigma_{sca} + \sigma_{abs} \tag{2.1}$$

Where σ_{ext}, σ_{sca} and σ_{abs} are the extinction, scattering and absorption cross-section, respectively. Both absorption and scattering process occurred simultaneously, but, there are circumstances where either one of the two process be in charge of. Comparing small particles (particle radius $a \ll \lambda$) with the wavelength, only absorption process is remarkable. Based on equation for dielectric constant;

$$\varepsilon(\omega) = \varepsilon'(\omega) + i\varepsilon''(\omega) \tag{2.2}$$

Where ε' and ε'' are the real and imaginary part of dielectric function of metal nanoparticles, respectively, and ω is the angular frequency of the exciting radiation, based on Drude's model (Kittel, 2005). From the assumption that the sphere particles with small sizes, embedded in an isotropic and non-absorbing medium with dielectric constant,$\varepsilon_m = n_m^2$, Mie explained the extinction cross section of the solutions where its real part is given by (Mie, 1908);

$$\varepsilon(\omega) = 9\frac{\omega}{c}\varepsilon_m^{\frac{3}{2}} V_o \frac{\varepsilon''(\omega)}{[\varepsilon'(m)+2\varepsilon_m]^2+\varepsilon''(m)^2} \qquad (2.3)$$

Where V_o is the volume of spherical nanoparticle, c is the velocity of light and ε_m is the dielectric constant of the medium. This equation explain the line shape of the absorption band of the particles. Considering the shape of nanoparticles is not confined to spherical shape, this theory had to be prolonged for another metallic forms.

2.1.1.2 Drude's Theory

Earliest 1900, a German physicist named Paul Drude has figured out a new theory of electrical and thermal conduction of metals. The theory describes a kinetic theory of gases to metal, considered as a gas of electrons. Drude assumed that the conduction of electrons in metal can be considered as molecules (Figure 2.1).

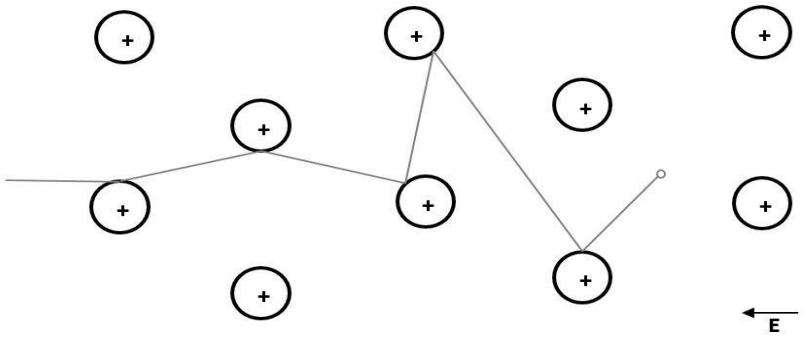

Figure 2.1: Drude's model of electrons bounced uniformly between heavy and stationary ions

Based on the free electron model, the dielectric function of free electron gas is denoted as:

$$\varepsilon(\omega) = 1 - \frac{n_e^2}{\varepsilon_o m \omega^2} \tag{2.4}$$

Where n_e is the electron density, ε_o is the vacuum permittivity, e and m are the electron charges and mass, respectively.

Meanwhile, plasma frequency of medium which have equal concentration of positive and negative charge can be denoted as:

$$\omega_p^2 = \frac{n_e^2}{\varepsilon_o m} \tag{2.5}$$

Thus, reconstructing equation of dielectric function of free electron gas;

$$\varepsilon(\omega) = 1 - \frac{\omega_p^2}{\omega^2} \tag{2.6}$$

Additionally, a constant offset, ε_∞ is introduced, which adding the effect of interband transitions at frequencies above plasma frequency, which not involving Drude model, thus, the dielectric function is represents as;

$$\varepsilon(\omega) = \varepsilon_\infty = \frac{\omega_p^2}{\omega^2} \tag{2.7}$$

2.1.2 Surface Plasmon (SP) and Surface Plasmon Resonance (SPR)

A charge density oscillation which also known as plasma oscillation can be excited on the metal-dielectric interface when react with light source. The free negatively charged electron is balanced by positive ions lattice in equilibrium condition. Because of the extremely large mass of positive ions when compared to the free electrons, the electron get replenish by the positive ions background. The attraction performs as a driving force

for the electrons as they move to positive region and assemble with higher density in order to obtain neutral charge. As a result, two forces are produced which are attractive force and repulsive force and set-up a longitudinal oscillations among the electrons (Sharma, Jha, & Gupta, 2007).

These oscillations are known as surface plasmons (SP) and the excitation occurred when the wave-vector of the light is same with the energy or momentum at the interface. Because of the electromagnetic field changed promptly, a surface plasma wave (SPW) was produced and travels through the interface, causing the field amplitude to decays exponentially in both medium. The field amplitude in metal (curve (b)), decay faster than the amplitude in dielectric medium (curve (a)) as depicts in Figure 2.2. In addition, the waves are transverse magnetic (TM) polarized and only get excited with the TM polarized light as they cannot be excited by direct beam of light (Srivastava & Gupta, 2013).

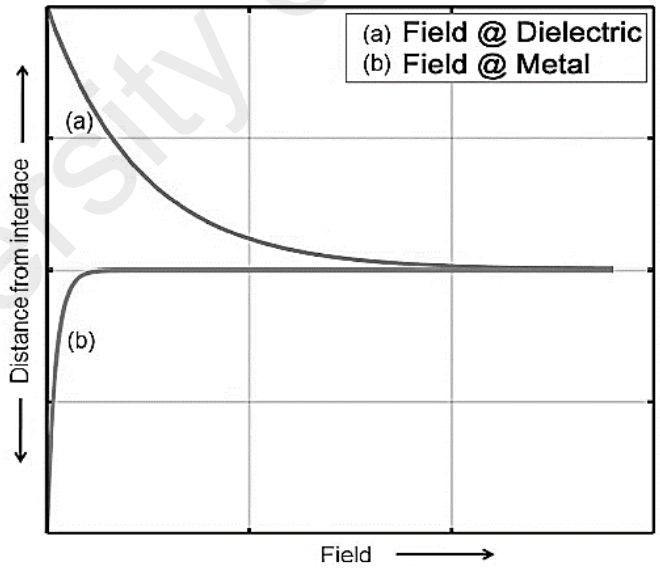

Figure 2.2: Variation of SP wave across the metal-dielectric interface (Srivastava & Gupta, 2013)

Surface plasmon resonance (SPR) is the resonance condition when evanescent wave relocate its energy to the surface plasma wave (SPW) and resulting the reflected light intensity to decline from the base of prism. This condition happens at a particular angle of incidence called the resonance angle, θ_{res} as shown in Figure 2.3 (Mishra, Bhardwaj, & Gupta, 2015). In addition, SPR angle is reliant on the refractive index of the material near the metal surface and plasmon cannot be established if the change in refractive index of sensing medium is small (Nguyen, Park, Kang, & Kim, 2015). The resonance condition can be happened depend on several criteria which are refractive index of prism, dielectric constant of the metals and also wavelength of the incident light (G. Gupta & Kondoh, 2007).

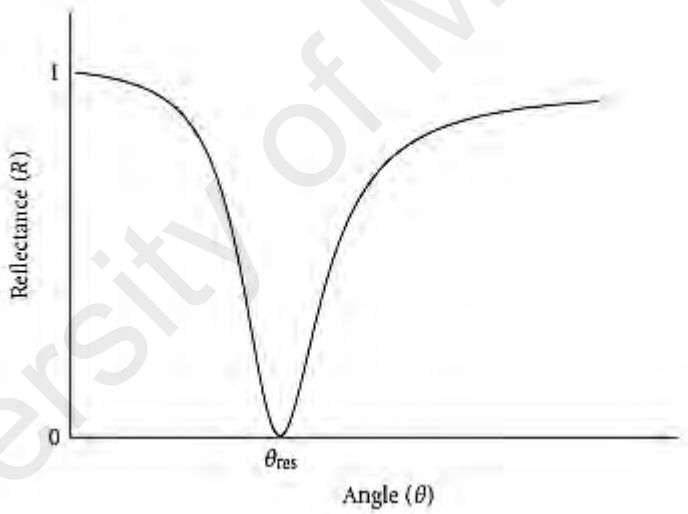

Figure 2.3: Spectrum of SPR (B. D. Gupta & Verma, 2009)

2.1.3 Localized Surface Plasmon Resonance (LSPR)

Localized surface plasmon resonance (LSPR) is an optical phenomenon created by trapped light wave in conductive nanoparticles (NPs) with dimension less than the wavelength of light. LSPR is differ compared to SPP which lossy waves are propagating along the metal surfaces. In addition, the localized plasmon oscillation is formed by the interaction of incident light and electron in conduction band of metal with a resonant

frequency that fully depends on the size and geometry, dielectric environment, composition, and also the separation distance between NPs (Caucheteur et al., 2015). Since there is no momentum carried out by the localized SPs, no momentum matching is necessary and only required energy is needed to be matched for the excitation of the electrons (Martinsson, 2014). Drude's model equation is used to prove the phenomenon of LSPR and the wavelength peak is totally depend on the dielectric function of a medium (Hong, Huh, Yoon, & Yang, 2012);

$$\varepsilon_r = 1 - \frac{\omega_p^2}{\omega^2+\gamma^2} \tag{2.8}$$

Where;

ε_r = real part of the complex dielectric function of the plasmonics material,

ω = angular frequency of the radiation,

ω_p = plasma frequency and

γ = damping parameter of the bulk metal

The LSPR are supported by many features of structures and there are few factors that affect the LSPR modes such as size, shape and distributions of particles (Murray & Barnes, 2007). It was proved that particles may formed to variety of shapes from the simplest form which is sphere to the complex form including ellipsoids, rods, stars, cubes and other possible shapes. Other than that, resonance behavior and localized modes can be achieved from the interaction between particles and also from the particles distributions that have specific inter-particles distance.

The size of particles influence the optical absorption and scattering, which the absorption takes place in small particle size as the plasmonics resonance is influenced by the dipolar component (Yockell-Lelièvre, Lussier, & Masson, 2015). It has been reported that small metallic particles contribute to maximum enhancement for visible detection. Meanwhile, as the particle size increases, scattering effects act as dominant contribution to the optical extinction, expecting a change in position and width of LSPR (Fernando, Semendy, & Wijewarnasuriya, 2012).

Another factor that influenced the LSPR mode is the particle shapes. Many researchers have reported the optical studies of particles with different shape and development of variety methods for the fabrication of the nanostructures. The fabrication methods of the nanostructures generally involving either growing the particles from a solution, such as electrochemical deposition (Zakaria et al., 2017) or lithography techniques (Mendes et al., 2004; Scuderi et al., 2016), where a material is deposited through a patterned mask. The factor of having different shapes of particle is important in order to optimize the localization and enhancement of the field correlate with the LSPR. The particle structures were designed with characteristics of inhomogeneous or sharp geometry, such as core-shell configurations or prisms, cube, and star-shaped nanoparticles (Nehl, Liao, & Hafner, 2006; Q. Wang et al., 2011).

In tuning LSPR modes, interaction between particles separated by small distances is very important. The distances are typically within the decay length of the electromagnetic field correlate with the mode. The energy modes with different EM field distributions produced from the hybridization effect that arise from coupling between LSPR modes (Murray & Barnes, 2007). Important reason of having small distance between particles is that strong enhancement in EM field are expected to occur within the gap between the particles (Kinnan & Chumanov, 2010).

2.2 Metallic NPs Materials

Metal NPs have been an interest for the researchers because of their unique properties, physically and chemically compared to their bulk properties. The most captivating features of the nanoparticles is their optical properties. Metals in nanoscale measurement perform high absorption in visible region of the spectrum and this absorption gives an attribution to the oscillation of conduction band electron with response to the electromagnetic (EM) radiation of light. In addition, the optical properties of metal nanoparticles can be modified in a controlled environment by adjusting the characteristics of the structure. The color and SP absorption band are strongly depend on the shape of the nanoparticles as they dependent on the size of them (J. Z. Zhang & Noguez, 2008).

Metallic NPs that have a strong interaction with the light are most likely used in plasmonics applications such as aluminum (Knight et al., 2014), silver (Liu et al., 2015), gold (K.-S. Lee & El-Sayed, 2006) or copper (Thi My Dung, Thi Tuyet Thu, Eric, & Mau Chien, 2011). Most of the metals, like silver and aluminum, appear in bright silvery when exposed to direct light since they are highly reflective across the visible spectrum. Meanwhile, metals like gold and copper are colored due to the inadequate reflection of high-frequency component of light, and the perceived light consist of predominant colors in the range of yellow to red wavelength.

Silver nanoparticles are most likely used in visible frequencies applications due to its small loss factor, contrastingly, gold is approximately to have three times more loss than silver. However, gold is usually preferred since it provides a better performance in many fabrication techniques and also gives a good stability against environmental degradation compared to silver, such as oxidation (Cai & Shalaev, 2010). Copper and aluminum are preferred to be used as industrial materials such as coating, electrodes and sensor elements. However, these noble metals are less favorable as plasmonics devices due to

the high oxidation and corrosion of copper films and also low sensitivity showed by aluminum. Still, these metals can be used in plasmonics application but they need to be support with another metal layers (Mitsushio, Miyashita, & Higo, 2006).

2.3 Enhancement of Optical Performance using Titanium Oxide (TiO_2)

Titanium oxide (TiO_2) is an *n*-type semiconductor that being considered because of the well-known properties, such as chemically stable, have a wide band gap and high dielectric constant and also a high refractive index. Because of these benefits, TiO_2 become a promising material for many application including sensing applications (Shukla et al., 2012; R. Viter et al., 2012; Z. Wang et al., 2011). This material appears in three phases; anatase, rutile and brookite (Hou, Zhuang, Zhang, Zhao, & Wu, 2003) and TiO_2 with anatase phase showed a good capability in water adsorption (Chen & Lu, 2005) among the three phases. Anatase phase of TiO_2 consist of crystalline structure that correlate to the tetragonal system and this is similar for TiO_2 with rutile phase, but differed with TiO_2 with brookite phase since in this phase, the structure of TiO_2 particles consist of orthorhombic crystalline (Malekshahi Byranvand, Nemati Kharat, Fatholahi, & Malekshahi Beiranvand, 2013).

It is substantial to have TiO_2 in nanometer size since TiO_2 with small size will result in the shifting of absorbance edge and the appearance of photoluminescence (PL) intensity peak (R Viter et al., 2011). It was reported that TiO_2 has a good adsorption behavior, thus, becomes a strong reason for its application in humidity measurement (Aneesh & Khijwania, 2012). Many techniques have been developed for the synthesis of TiO_2 nanoparticles, such as hydrothermal (Andersson, Österlund, Ljungström, & Palmqvist, 2002), solvothermal (Wahi, Liu, Falkner, & Colvin, 2006), emulsion precipitation (Ramakrishna & Ghosh, 2003) and sol-gel process (Bessekhouad, Robert, & Weber, 2003).

2.4 Basic Study of Plasmonics Optical Fiber Sensor

In recent years, many researchers are concern on the merging of optical fibers and nanotechnologies specifically integrating plasmonics nanoparticles on the active area of the optical fiber as a sensor. Development of surface plasmon resonance (SPR) sensors have gain an interest since number of reporting publications on the applications of SPR sensor for medical diagnostics, food safety monitoring and environmental monitoring has been expending expeditiously. In 1902, Wood was the first person who discovered SPR and observed that an anomalous pattern of dark and bright bands appeared in the reflected light when polarized light was directed onto a mirror with diffraction grating on its surface (Wood, 1902).

Combination between fiber optic and plasmonics shows a great potential in sensor application as the optical fiber have high resistance to electric shocks, immune to radio frequency and electromagnetic interference, act as remote sensing and also low cost for some cases (Kude & Khairnar, 2008). Moreover, this technique is feasible due to the changes of refractive index which can be detected in a short time without any delay. The combination between optical fiber and SPR technique is based on a theoretical reason that direction of light rays in optical fiber is based on total internal reflection (TIR).

Total internal reflection (TIR) occurred inside the core of the fiber when light rays propagate and incident at one end of the fiber. In this condition, the light ray does not return from the interface but preferably return after penetrating in medium which has lower refractive index. This result may due from the creation of evanescent field which excites surface plasmon at the metal surface. The wave equivalent to this evanescent field is called evanescent wave which is produced when the light beam incident on the dielectric-metal interface with certain angle, θ. The excitation of surface plasmon happens

when evanescent wave is phase match with that of SPs of same frequency at specific angle of incidence, θ_{res} (B. D. Gupta & Verma, 2009).

The pairing between evanescent fields with surface plasmons relies on the wavelength of the light, parameter and geometry of the fiber and also properties of the metallic layer. Single-mode fiber and multi-mode fiber have different pairing mechanism due to their various mode transmission properties which depends on the number of modes. In addition, different types of fiber (tapered and straight) will demonstrated different power of light coupling due to the geometrical configurations (Sharma et al., 2007). At sensing medium, if the refractive index of the dielectric medium is altered, the dip position in the transmission spectrum will altered as well (Srivastava & Gupta, 2013).

2.4.1 Types of Optical Fiber used as Sensor

Typical optical fiber sensor based on SPR offers many unique advantages as mentioned earlier but there are two problems exist in the development of the sensor. The first problem is phase matching between waveguide core mode and plasmonic wave and the second problem that have attract the researchers is the process of metallic layer coating into a sensor to excite SPR wave (Tian, Lu, Chen, Lv, & Liu, 2012). In order to create evanescent field so that the SPR wave can be excited and the fiber can perform as a sensor, part of the fiber must be unclad. To resolve the problems, many approaches have been proposed to modify the fiber such as tapered fiber (Jha, Verma, & Gupta, 2008), D-shaped fiber (Tian et al., 2012), exposed core microstructured fiber (Klantsataya, François, Ebendorff-Heidepriem, Hoffmann, & Monro, 2015) and hetero-core structure fiber (Iga, Seki, & Watanabe, 2004).

2.4.1.1 Side Polished Optical Fiber

The structure of side polished optical fiber is shown in Figure 2.4. This optical fiber also called as D-shaped optical fiber due to the formation of cross-sectional D shape structure as one side of the fiber after it had been polished. This fiber is produced by the process of mechanical polishing and chemical etching. The creation of high evanescent field makes the propagation constant of the fiber become more responsive to the surrounding refractive index (Liao et al., 2016). In addition, optical transmission attenuation is caused by the interaction of evanescent wave on the surface of the fiber with the surrounding environment (De-Jun, Mao-Sen, Liu, Xi-Lu, & Dong-Fang, 2014). It is reported that when the light rays coupled out from the polished fiber into coated metallic nanostructures film, the active surface area can be increased by several level of magnitude (Y. Zhang, Gu, Schwartzberg, & Zhang, 2005).

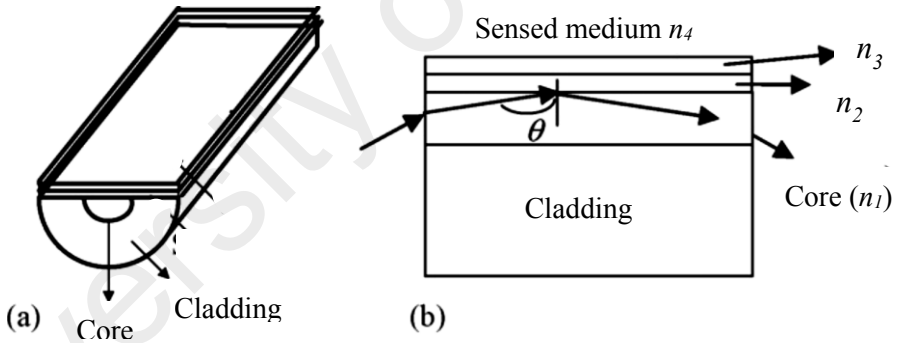

Figure 2.4: SPR D-shaped fiber sensor (Chiu, Shih, & Chi, 2007)

2.4.1.2 Tapered Optical Fiber

Tapered optical fiber or often known as micro optical fiber has been used intensively in complex photonics application such as super continuum generation, harmonic generation and also sensors. A wide range of techniques were used in the fabrication process of the tapered fiber; laser ablation (Morales & Lieber, 1998), fiber pulling

(Clohessy, Healy, Murphy, & Hussey, 2005) and the most versatile technique is flame heating technique (Harun, Lim, Tio, Dimyati, & Ahmad, 2013).

The fabrication is done by stretching a conventional optical fiber until the core and cladding diameter are reduced (Figure 2.5), resulting the evanescent fields to spread out (H.-Y. Lin, Huang, Cheng, Chen, & Chui, 2012). Although tapered fiber have been reported to have higher fractional power around the fiber waist compared to the exposed core fiber (Grazia, Riccardo, & Ciaccheri, 1998), controlling the thin films (used to excited SPR) coated on the whole fiber waist region was totally difficult and complicated to handle (H.-Y. Lin et al., 2012).

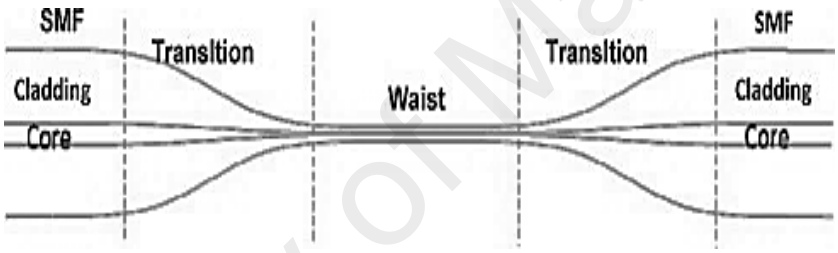

Figure 2.5: Configuration of tapered optical fiber (Harun et al., 2013)

2.4.1.3 Hetero-core Structure Optical Fiber

Hetero-core structure optical fiber has been approached by many researchers as a probe in sensing applications. The configuration of this fiber consists of two fibers with different core diameter, connected by thermal fusion splicing (Sharma et al., 2007). The most used scheme (Figure 2.6) consists in splicing a single mode fiber (SMF) between multimode fiber (MMF) as reported (Iga et al., 2004; Takagi, Sasaki, Seki, & Watanabe, 2010). The core mismatch between the fibers used caused a leakage of transmitted power into cladding of small core diameter fiber, and this were intentionally done so that an optical evanescent wave may be excited (Caucheteur et al., 2015). This fiber configuration are reported to be the most efficient configuration in terms of power budget and cost.

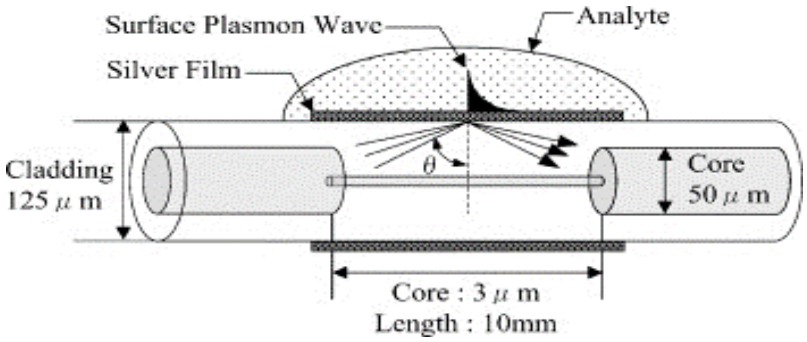

Figure 2.6: Structure of hetero-core fiber (Iga et al., 2004)

2.4.2 Review on Humidity Sensor

Table 2.1 shows the scheme of proposed humidity sensor based on previous work. Previously, these three types of optical fiber were commonly used by the researchers as a plasmonics humidity sensor since the fabrication process of the fiber is low cost and simple.

Table 2.1: Humidity optical fiber based sensor schemes proposed from literature review

Types of optical fiber	Fabrication technique	Structure of humidity sensor	Sensing material	Range of humidity (%RH)	Sensitivity
Side polished optical fiber	Mechanical polishing and chemical etching	Side polished single mode (Huang et al., 2018)	Graphene oxide	58.2 – 92.5	0.427 dB/%RH
		Side polished single mode (Ouyang et al., 2017)	Molybdenum diselenide ($MoSe_2$)	32 - 73	0.321 dB/%RH

Table 2.1, continued

Tapered optical fiber	Laser ablation, fiber pulling and flame heating technique	Biconically tapered single-mode optical fiber (Bariáin, Matías, Arregui, & López-Amo, 2000)	Hydrophilic gel (agarose)	30 - 80	6.5 dB/%RH
		Tapered fiber Bragg grating (FBG) (Aris et al., 2017)	Zinc oxide	55 - 80	0.089 dBm/%RH
Hetero-core structure optical fiber	Thermal fusion splicing	Single mode side polished – multimode – singlemode (Wang et al., 2018)	Uncoated	30 - 90	0.069 dB/% RH
		Single-mode - no-core - single-mode fiber (W. Xu et al., 2017)	Agarose gel	30 - 75	-0.075 dB/%RH

CHAPTER 3: RESEARCH METHODOLOGY

3.1 Introduction

This chapter presents the technique used in completing experimental work. The chapter will discuss on technical work for the optical characterization of Ag with arbitrary shapes. The preparation of substrates used to deposit Ag nanostructures and the deposition process will be discussed in this section. The equipment used to characterize the optical properties of Ag nanostructures is also mentioned in this section. The following section will discuss on the formation of Ag nanoparticles using electron beam evaporation system. This section is also mentioned the preparation of TiO_2 solution, which introduced as another layer, covering the Ag layer. In part C, the preparation of side polished optical fiber and the fabrication process of optical fiber sensor with integration of Ag/TiO_2 nanoparticles as a humidity sensor are explained.

3.2 Part A: Optical Characterization of Silver (Ag) with Arbitrary Shapes

Figure 3.1 illustrates the flow chart for the preparation process of Ag nanostructures with arbitrary shapes using electrochemical deposition technique.

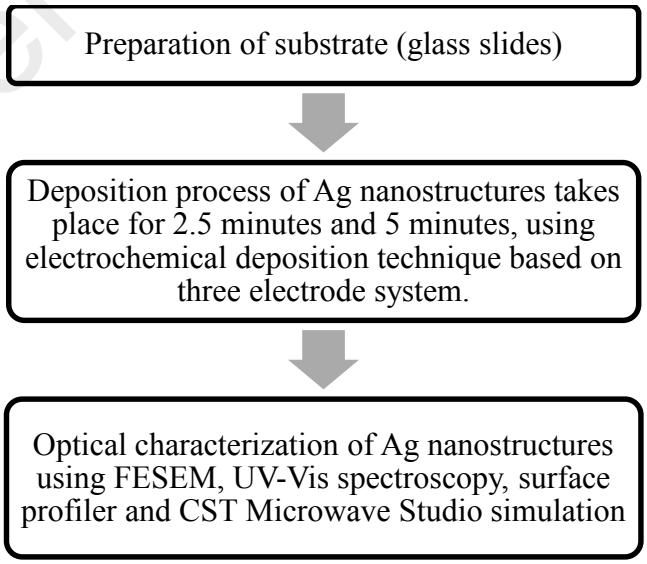

Figure 3.1: Flow chart diagram illustrates the process in preparing Ag nanostructures with arbitrary shapes

3.2.1 Preparation of Substrate

A clean glass slide was used to provide a flat platform for the polished fiber and to prevent the fiber from break throughout the experiment since the polished fiber is fragile. The glass slide was cut into small size (2.5 × 2.5 cm) to ease the polishing process.

The process of cleaning glass substrate starts by immersing the glass slide in a beaker containing mixed solution of DI water and deform soap water with ratio of 2:1. The glass substrates was sonicated for 15 minutes and rinsed with DI water, acetone and ethanol respectively. The substrate was rinsed again with DI water before dried using nitrogen blow.

3.2.2 Deposition Process of AgNPs

In this part, silver nanoparticles (AgNPs) were deposited on glass surface using electrochemical deposition technique. This technique is one of the industrial process and was used to deposit the particles contained in a solution onto a substrates under the influence of an electric field. Materials with colloidal particles usually used in this deposition technique as they can carry a charge and these materials include metals, polymers, ceramics, dye and pigments.

A three-electrode electrochemical cell and silver-ammonia ($[Ag(NH_3)_2]OH$) solution were used to conduct the deposition of AgNPs. Firstly, silver ammonia solution was prepared by mixing ammonia (1 wt %) with 10 mL of 50 mM $AgNO_3$ solution. The solution mixture was stirred until the color of the solution changed lighter which altered the concentration of $[Ag(NH_3)_2]OH$ solution to 40 mM (Pavaskar, Theiss, & Cronin, 2012). The three-electrode system used is described in Table 3.1 and the schematic diagram of the system is shown in Figure 3.2.

Generally, there are two methods of electrochemical deposition; i.e, cyclic voltammetry (CV) and chronoamperometry (CA), both are carried out in a prepared solution using a potentiostat/ galvanostat (Versastat 3 Applied Research Princeton, USA). CV is used to determine suitable potential for this study. The potentiostat worked back and forth and was applied onto the working electrode to produce a voltammogram, which also known as a scan (Daubinger, Kieninger, Unmussig, & Urban, 2014). After few cycles, an optimum potential of 0.6 V was used to deposit AgNPs on the glass substrates using the CA electro deposition technique. Two deposition times were set as 2.5 min and 5 min.

Table 3.1: Three-electrode system for the electro deposition technique to coat AgNPs

Materials/ Substrate	**Function**
Glass slides (substrate)	Working electrode
Platinum nanowire	Counter (auxiliary) electrode
AgCl	Reference electrode

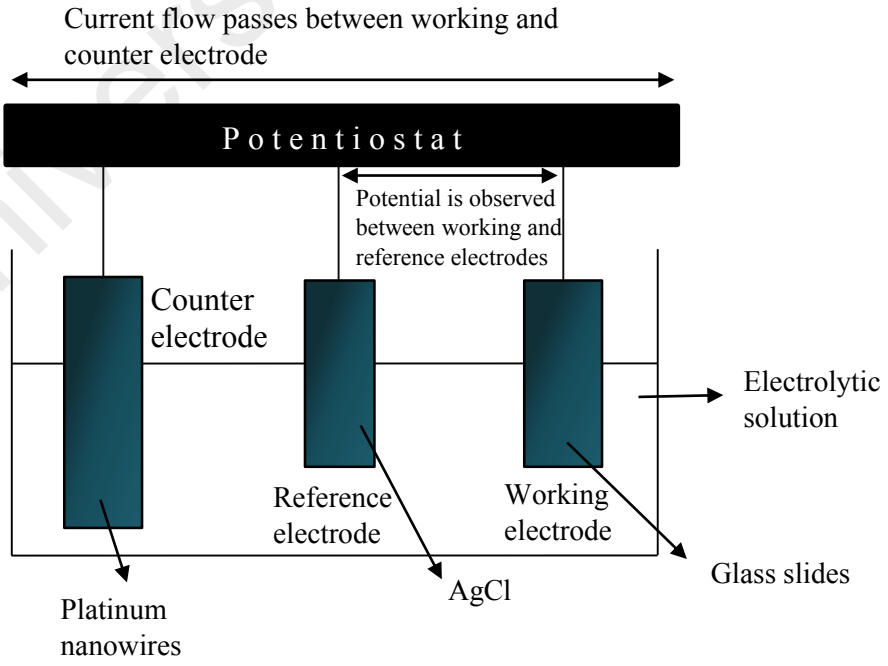

Figure 3.2: Schematic diagram of electrochemical deposition technique

3.2.3 Optical Characterization of AgNPs

Two important characteristics are considered in the study of the plasmonics, which is metal NPs structures and their plasmon resonance behavior. To emphasis this characteristics, imaging and scattering properties must be carried out. For the optical characterization of the deposited samples, further explanation on the equipment used has been discussed as below and parameters used for the characterization is shown in Table 3.2.

3.2.3.1 Field Emission Scanning Electron Microscopy (FESEM) Imaging

To characterize the surface morphology of the samples, a Quanta 400F scanning electron microscopy (FESEM) was used to obtain high resolution images of the Ag structures down to nano-scale measurements. FESEM imaging technique is frequently used to study the morphology of microstructures and thin film fabrication. Similar to normal SEM imaging, the aim of using FESEM imaging is to visualize the structures of tiny objects, but, the FESEM imaging is highly advance since it can capture the size of structures in nano scales.

The scanning magnification scale in FESEM image is used to determine the size of the particles and the film thickness is measured from the cross section of the FESEM image of the film samples. During the scanning process, electrons that generated from a source are focused by electronic lenses to create a confined beam that bombards the samples. The incident beam produces second electrons which cause a small energy loss and as a result, the electrons ionized in the atom of the samples. A detector captures the secondary electrons and generates an electronic signal which then is amplified and transformed to a digital image than can be observed on a monitor.

The quality of the images produced is rely on the conductivity of the samples, as the samples with non-conductive surface is hard to focus and thus, contribute to a low quality

image. Since the technique of FESEM imaging captures image using electron beams on the surface of the samples, charging might hit the non-conductive surface which will damage the samples. Therefore, adding a metallic layer such as gold and silver will help protecting the samples with non-conductive surface.

3.2.3.2 UV-Vis Spectroscopy

In this research, PERKIN ELMER LAMBDA 750 UV-Vis spectrometer was used to study the absorption properties of the samples. Spectroscopy is the technique used to analyze the interaction of electromagnetic radiation and use a range of ultraviolet and visible (UV-Vis). The light beam from UV and/or visible light source is divided according to the wavelengths by prism or diffraction grating. This technique determines the intensities of the light beams that passing through a sample *(I)*, and then compared with the intensity of the reference beam (I_0). The ratio of I/I_0 is named as transmittance which usually signified as %T. Absorbance A is related to transmittance as it presented as $A = \log\frac{I0}{I}$, meanwhile R% is the reflectance percentage gained from the ratio of the intensity of reflected light from a sample to the intensity of reflected light of a reflectance sample.

3.2.3.3 Surface Profiler

The fundamental of P-6 profilometer is based on the motion of diamond stylus, which physically moving a probe on the surface of a sample to measure the surface height and surface roughness of the sample. A KLA-TENCOR P6 surface profiler was used in this work to measure the thickness of the Ag nanoparticles deposited on the glass surfaces.

3.2.3.4 CST Microwave Studio Simulation

Computer Simulation Technology (CST) microwave studio is a simulation tool for the 3D EM design for components with high frequency. This simulation includes various different methods that have their own advantage, which are time domain solver and frequency domain solver, depends on the applications. In this work, CST Microwave

Studio 2016 with frequency domain solver has been used to simulate the nanoparticles to observe the absorption properties and electric field intensity distributions.

Table 3.2: Parameters used for the optical characterization of Ag nanostructures with arbitrary shapes

EQUIPMENT	PARAMETERS	SETTING VALUE
CST Microwave Studio simulation	Incident wave polarization	y-direction
	Wavelength (nm)	425
Field Emission Scanning Electron Microscopy (FESEM)	Magnification	×20 000, ×10 000, ×1000
	Vacuum mode	High vacuum
UV/VIS/NIR spectroscopy	Wavelength range (nm)	190 - 2000
	Light source	Tungsten-Halogen (Vis) and Deutrium (UV)

3.3 Part B: Optical Characterization of AgNPs and Titanium Oxides (TiO_2) Nanoparticles

Figure 3.3 illustrates the flow chart diagram for the preparation process of AgNPs and TiO_2 nanoparticles using electron beam evaporation technique (for Ag) and drop cast technique (for TiO_2).

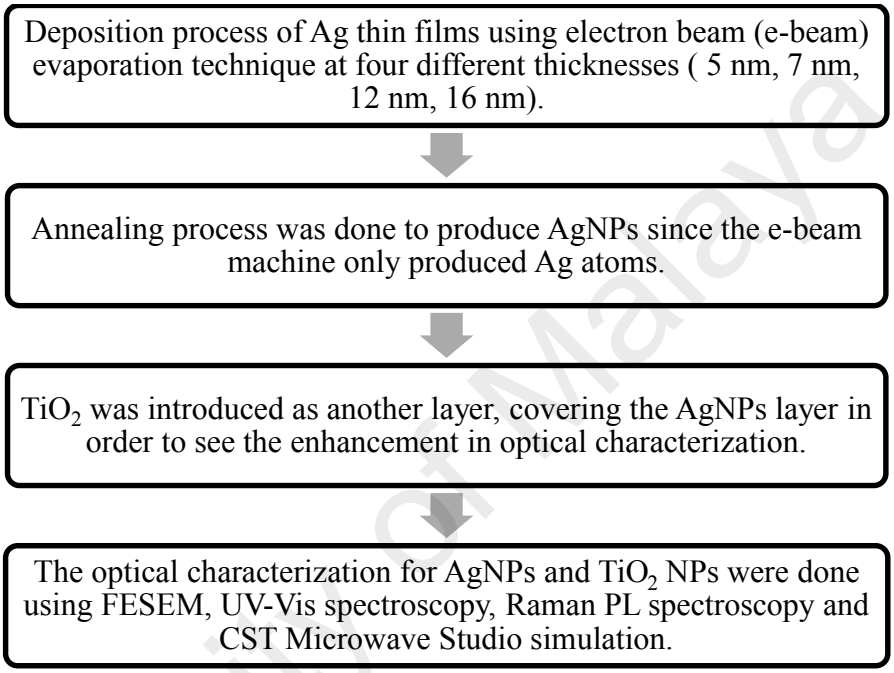

Figure 3.3: Flow chart diagram for the preparation process of AgNPs and TiO_2 nanoparticles on a glass substrate.

3.3.1 Deposition of AgNPs Thin Layer and TiO_2 Nanoparticles Solutions

3.3.1.1 E-beam Deposition

E-beam evaporation processes are categorized under physical vapor deposition along with other method such as sputtering, e-beam lithography and thermal evaporation. Throughout the study, an e-beam evaporation machine model EB43-T manufactured by Korea Coating Materials and Components (KCMC) was utilized to create thin film layer of AgNPs. The machine consists of two main parts, where a vacuum system is located at the first part and deposition system was placed in the second part of the machine as shown

in Figure 3.4. In order to operate well, both parts have their own components that perform an important task as discussed below;

a) Vacuum systems

This system is necessary at the beginning of the e-beam evaporation process, where the task is to pump the deposition chamber. This system consists of two components which are rotary pump (R/P) and turbo molecular pump (TMP). Rotary pump is the basic component for the system and has two functions, which are to starts the pumping process of the vacuum chamber from high atmospheric pressure and secondly, is to back pump the turbo molecular pump. However, the rotary pump in the e-beam evaporation machine is not strong enough to absorb the molecules from the atmospheric pressure inside the chamber (pump down reading is $\sim 1 \times 10^{-3}$mbar). Since the pressure of the surrounding chamber need to be pump down to $\sim 1 \times 10^{-7}$mbar, other high power pump is needed and this is where the turbo molecular pump starts to operate. The turbo molecular pump is a high speed pump with high speed of motor fan. Thus, only small molecules are allowed to be sucked out of the chamber as particles with big size may damage the fan blades of the pump.

b) Deposition systems

This system is located inside a chamber of the e-beam evaporation machine where all the deposition process take place here. Figure 3.5 illustrates the schematic diagram of the deposition system inside the chamber. A substrate are placed in a built- in substrate holder with position of facing downward and deposition metal components are located at the bottom of the chamber.

As deposition process started, the vacuum system starts to operate by pumping down the chamber until the reading of the atmospheric pressure inside the chamber reach $\sim 1 \times 10^{-5}$ to $\sim 1 \times 10^{-7}$ as interpreted earlier. In Figure 3.5, the function of tungsten filament is to emit the electrons with the help of high amount of current and voltage. When the electrons are emitted, a deflecting magnet will change the route of the electrons and transmit them directly onto a target deposition metal. The atoms of the target metals are transformed into gaseous phase which caused by the emitted electron beam and these gaseous atoms then coated the samples in the chamber.

The metal coating can be control based on the desired thickness using main shutter that is placed between the deposition target and substrate position. A thickness monitor was also included inside the chamber and it is connected to a programmed control unit and display screen so that the deposition rate (thickness (Å) / time (s)) and progressing deposition process can be monitored. The deposition rate can be adjusted by tuning the current flows. Still, some parameters need to be set before the samples being coated since different materials have different properties. As all parameters were set, the main shutter would open and deposition time starts to count synchronously. The shutter would close together with time counted stop immediately after gain the desired thickness of metal coating.

A clean glass substrate is placed in the substrate holder inside the vacuum chamber of the e-beam machine and pumped down at pressure of 1.7×10^{-5} mbar. The voltage and current used to generate electron beam was turned up to 7 kV and 120 mA, respectively after the pressure stable for about 40 minutes. The coating process was done for about 20 minutes and the thicknesses of Ag were sets to 5 nm, 7 nm, 12 nm and 16 nm. Using this technique, the thickness of metal layer can be controlled easily by the main shutter and this technique forms a smooth and uniform coating.

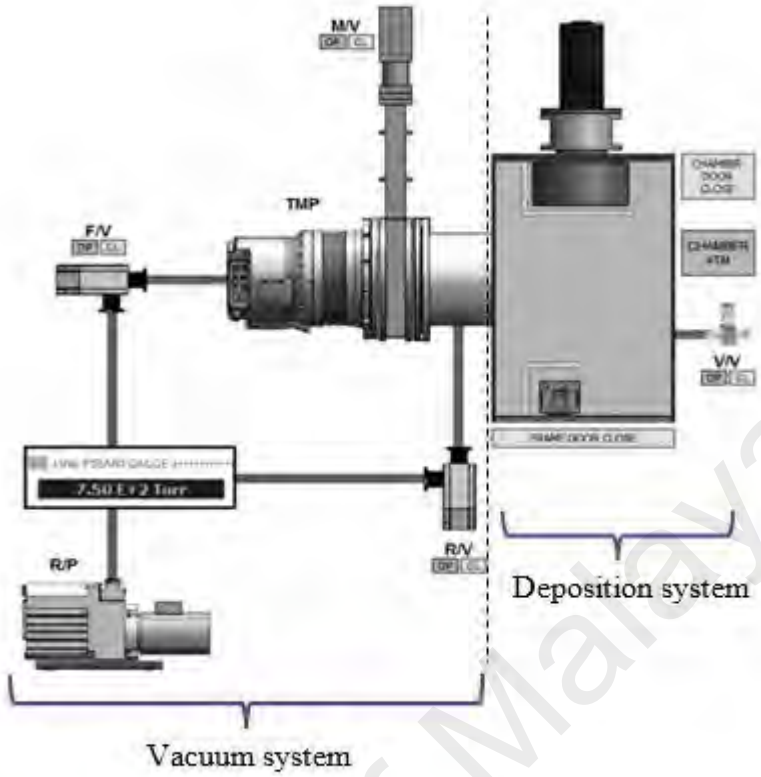

Figure 3.4: Schematic diagram of e-beam system used

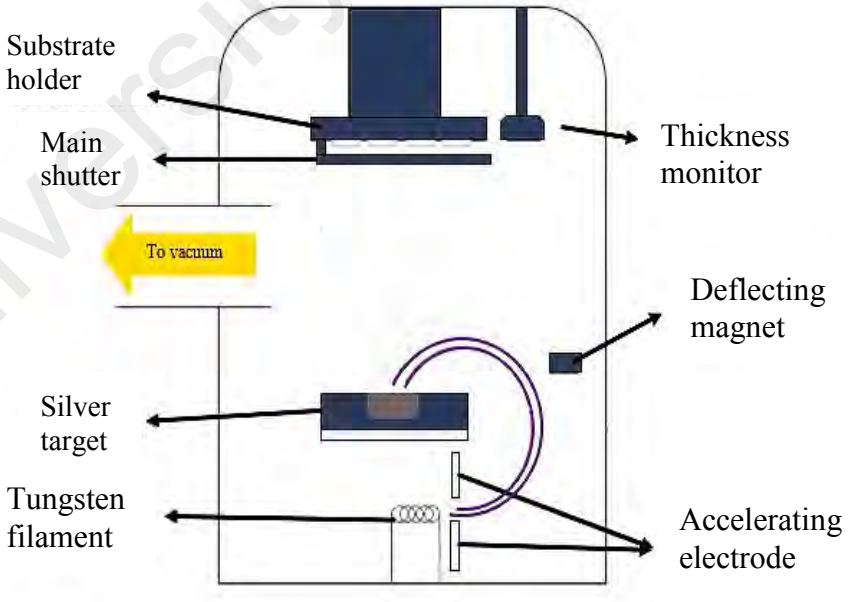

Figure 3.5: Schematic diagram of deposition process inside the vacuum chamber of the e-beam machine

3.3.1.2 Annealing Process

Followed by annealing process, this step involves the exposure of the metal thin layers to a certain temperature to form randomly distributed nanoparticles structures. The formation of nanoparticles is happened due to the surface tension created by the heating energy and also because of the recrystallization process that makes the size and distribution of nanoparticles to be randomly appeared. The coated fiber went through an annealing process for 2 hours with temperature of 170 °C.

3.3.1.3 TiO_2 as another layer

A metal oxide, specifically TiO_2 was introduced as another layer, covering Ag layers in order to enhance the performance of the metal nanoparticles as well as a protection to avoid oxidation from Ag thin layer. A commercial 99% pure TiO_2 nanoparticles of anatase phase were obtained in powder form. The TiO_2 solution was prepared by dissolving the anatase TiO_2 powder in deionized (DI) water with an assistance of sodium lauryl sulphate (SLS) solvent. Then, the mixture was stirred and sonicated for 30 minutes at 30 °C to ensure all TiO_2 powder dissolved completely in the solution. The metal oxide was deposited by dropping few drops of TiO_2 solutions, about 1500 µL on top of the metallic layer. The samples were then left to cure in open air environment for few hours until the solution completely dried.

3.3.2 Optical Characterization of AgNPs and TiO_2 NPs

Similar to previous part, the surface morphology of the AgNPs was observed using field emission scanning electron microscope (FESEM) images and energy dispersive X-ray spectrometer (EDS). Meanwhile, the optical characterization of the samples was observed using Raman photoluminescence (PL) and Raman UV-Vis. In this part, CST Microwave Studio was used to simulate AgNPs at different thicknesses to see the

performance of E-field for each of NPs. Further explanation on Raman PL spectroscopy is mentioned below and parameters of the measurement used are shown in Table 3.3.

3.3.2.1 Raman Photoluminescence (PL) Spectroscopy

Raman PL spectroscopy is used to measure the intensity of emitted electromagnetic radiation. The basic fundamental of this technique is based on the light absorption on a sample and transmit excess energy into a material, and this process is called photo-excitation process. The excess energy can be dissipated by the sample is by the light emission which known as luminescence, or photoluminescence. The intensity and spectral of photoluminescence gives an explanation on the interaction of electron-hole pair under a condition where emitted energy is in the form of photonic energy. In this work, PL measurement was intentionally done using Renishaw inVia Raman microscope to study the potential enhancement of TiO_2 nanoparticles coated on AgNPs.

Table 3.3: Parameters used for the optical characterization of AgNPs and TiO_2 NPs

EQUIPMENT	PARAMETERS	SETTING VALUE
Field Emission Scanning Electron Microscopy (FESEM)	Magnification	×60 000, ×120 000
	Vacuum mode	High vacuum
UV/VIS/NIR spectroscopy	Wavelength range (nm)	200 - 1000
	Interval time (ms)	5
Raman PL spectroscopy	Excitation wavelength (nm)	325
	Focused objective lens	20×
	Laser power (%)	100
	Exposure time (s)	10
CST Microwave Studio simulation	Frequency (Hz)	504.54 (5 nm)
		530.92 (7 nm)
		637.2 (12 nm)
		648.2 (16 nm)

3.4 Part C: Studies on Application of Optical Fiber as a Humidity Sensor

3.4.1 Preparation of Side Polished Optical Fiber

A single mode optical fiber (SMF-28, Corning) was used to fabricate sample of sensing probe in this study. The diameter and refractive index of the core is 8.2 µm and 1.4682 respectively, while the cladding, with the diameter of 125 µm with lower refractive index, 1.444 at 1550 nm. The process of fabrication starts by polishing a cleaved fiber using polishing film repeatedly. The setup for polishing process was shown in Figure 3.6. A fine polishing sandpaper sheet was mounted on the polishing machine to polish the fiber until part of cladding was removed and then, 0.02 µ Final Polishing Lapping Film is used to get a consistent and smooth surface of the polished region. Several repetitions of this stage may be needed as the fiber is polished manually and it was easily break as the cleaved fiber is fragile.

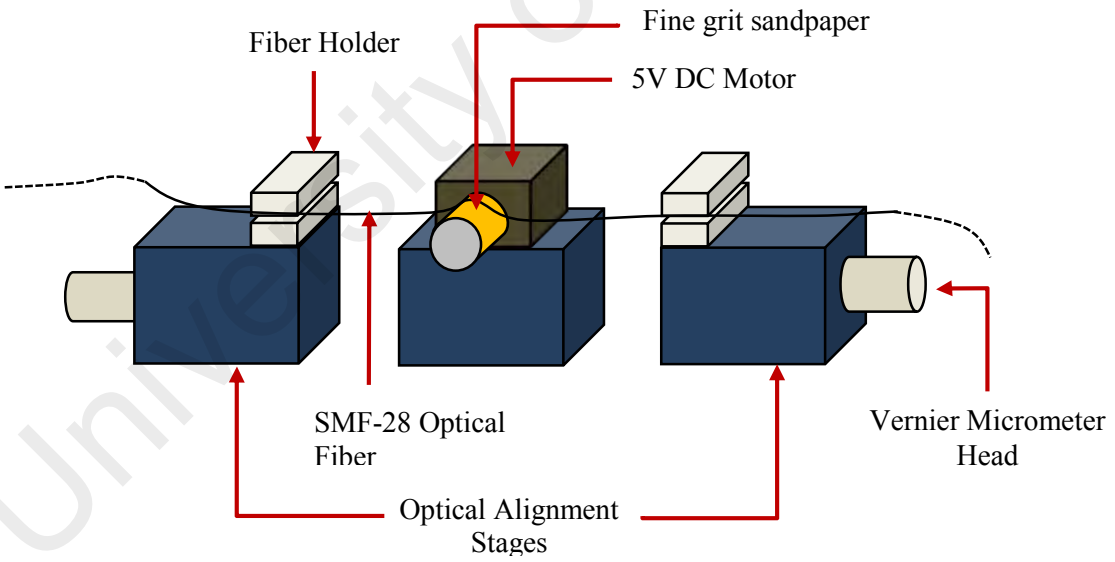

Figure 3.6: Experimental setup of polishing process

The process will end after the desired polishing depth is determined. The determination of polishing depth is observed manually from a leakage of red light during polishing process. Red light was fired to the optical fiber during the polishing process and once the leakage of light is observed as shown in Figure 3.7, the process has to stop. The polished

core is observed using an optical microscope to see the structure of the fiber (Figure 3.8). The loss in output power of the fiber is measured before and after polishing process by connecting optical power meter to the output of the fiber to get better estimation of the actual depth of polished core.

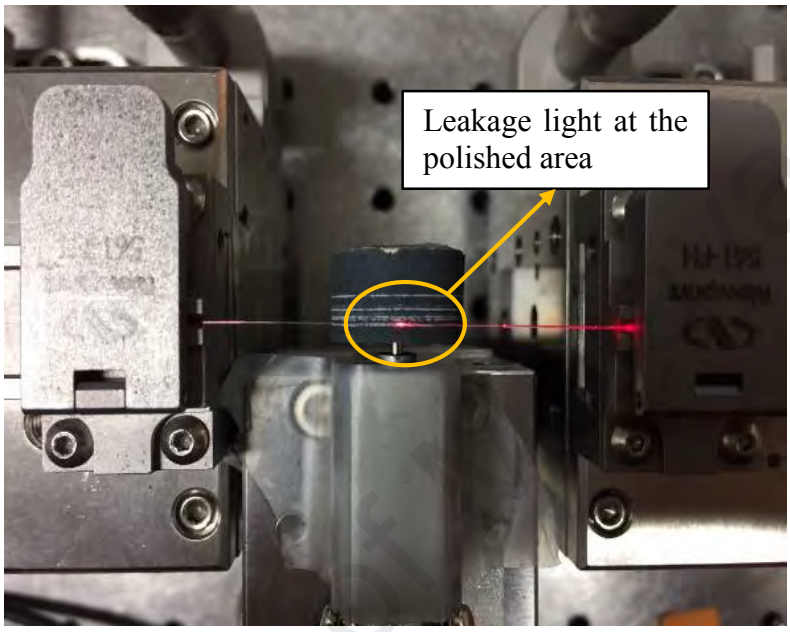

Figure 3.7: Condition of side polished fiber after polishing process

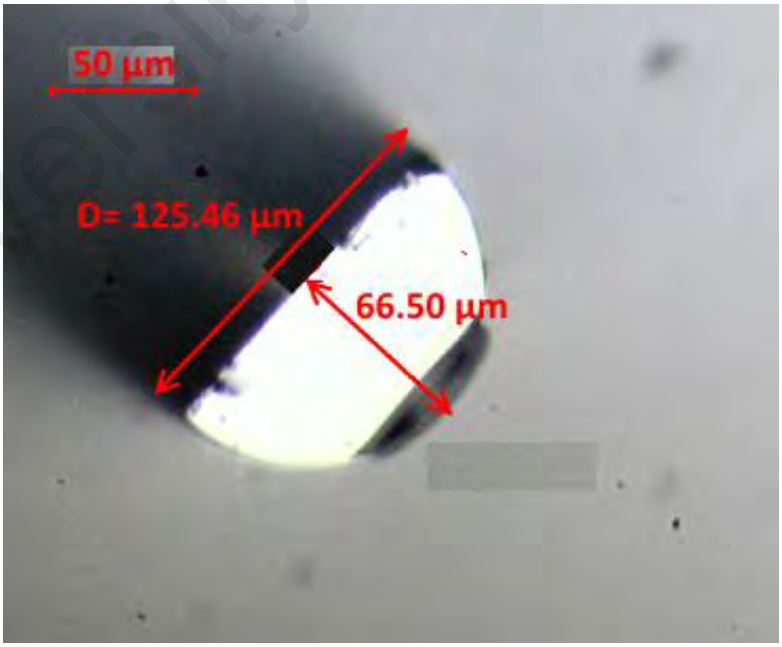

Figure 3.8: Microscope image of side polished optical fiber from end view

Figure 3.9 shows the graph of the output power before and after polishing process. In the graph, the loss in power is about 1.18 dBm which gives a good indication for the fiber as a sensing probe. The significant of polishing the core to about half of the diameter is to ensure the evanescent wave can be excited at the sensing region. Length of polished area is estimated to be 5 mm, which is the active area of this probe. The polished fiber was placed on the clean glass slide using epoxy and was left under open air environment for curing process before went through the deposition process of AgNPs and TiO_2 NPs.

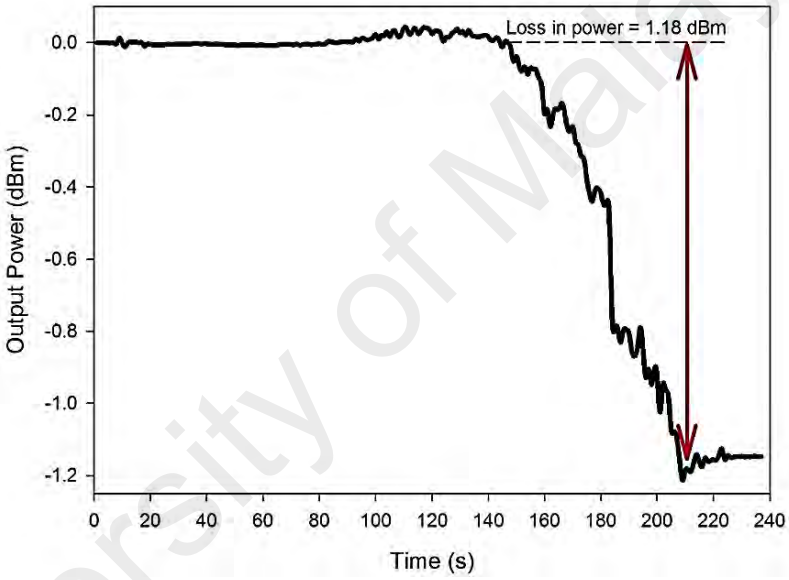

Figure 3.9: Loss in output power after polishing process

3.4.2 Experimental Setup for Humidity Sensor Characterization

The samples of side polished optical fiber including uncoated fiber, Ag coated fiber, and Ag/ TiO_2 coated fiber were fabricated using e-beam evaporation technique (for Ag) and drop cast technique (for TiO_2) to observe the response of the sensors in an environment with variable parameters. The fabricated sensor was characterized using ASE broadband light source together with an optical spectrum analyzer (OSA). An optical power meter was used to study the resonance peak wavelength and also output intensity power. The arrangement is shown in Figure 3.10. One end of the fiber sensor was connected to the optical white light source and another end of the fiber was connected to

the OSA with tunable wavelength range of 600 to 1600 nm. For characterization of humidity sensor, the sensor was placed in a small chamber. A reference hygrometer was attached to the chamber to monitor the absolute values of the relative humidity (%RH) ranged from 50 to 90 RH%. During the experiment, the %RH inside the chamber was controlled using saturated salt solution, sodium hydroxide (NaOH) specifically. All experiments were conducted at controlled room temperature, which was ~ 25 °C.

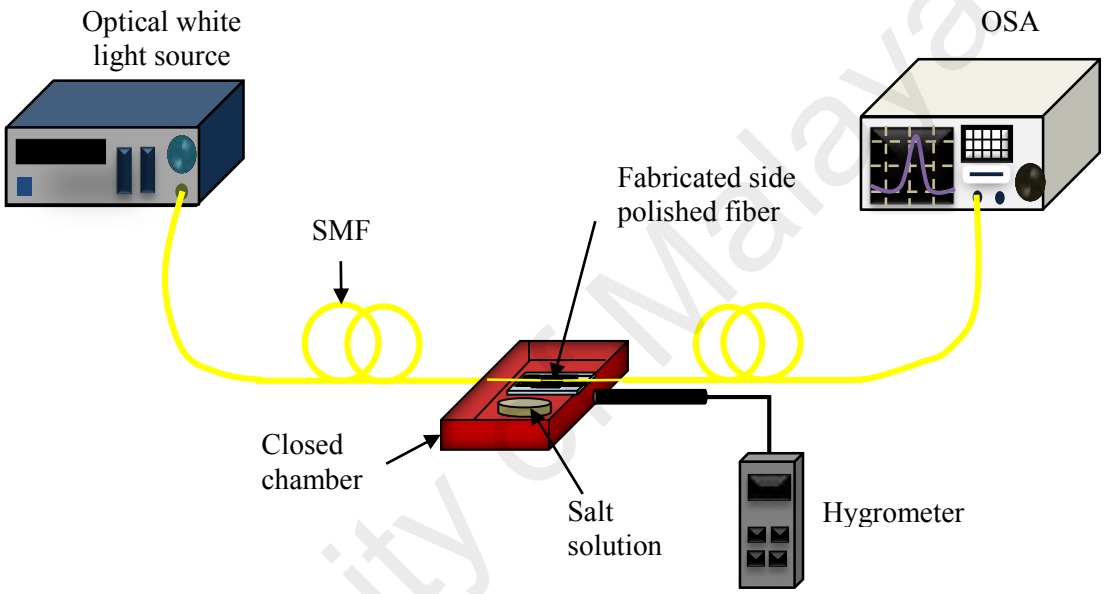

Figure 3.10: Experimental setup for humidity sensor

CHAPTER 4: RESULT AND DISCUSSION

4.1 Introduction

This chapter presents the studies of optical properties and morphology characterization of Ag structures. The first section in this chapter will discuss the surface morphology of Ag with different shapes such as microflowers and hexagonal structures which we defined as arbitrarily shapes. These structures were formed through electro deposition process which will be elaborated more in this section. The following section will discuss on the formation of Ag nanoparticles using electron beam evaporation system. The investigation is based on the size of Ag nanoparticles as this will give optimum plasmonics behavior which will be favor to be implemented in the fabrication of the optical fiber sensor. The Ag used commonly known as a material which is easily been oxidized; therefore in this section we introduce the combination of TiO_2 for better device performance. In part C, the fabrication of optical fiber sensor with integration of Ag nanoparticles as a humidity sensor from the linearity and sensitivity achievement is explained. Part A and part B sections portrayed the simulation studies using CST Microwave Studios 2016 to observe the agreement between experimental and simulation findings. The simulation studies are crucial as it gives overall view on the effect of this structures from optical properties and electromagnetic field distribution.

4.2 Part A: Optical Characterization of Silver (Ag) with Arbitrary Shapes

4.2.1 Surface Morphology of Ag structures

SEM images of Ag structures are shown in Figure 4.1 at deposition times of 2.5 minutes and 5 minutes as both times are an appropriate time for the structures to fully form. In Figure 4.1(a – c) shows the initial process started with small sizes of Ag structures appear on the glass substrate. The deposition time recorded as 2.5 minutes depicts the hexagonal structures with height of the structures is 234.84 nm ~ 235 nm (shown in Table 4.1). This structures are slowly vanish after deposition time of 5 minutes. This morphology are likely due to the Ag particles are deposited at the same area repeatedly with the high density of particles. The formation is deliberately becomes micro/scales size flower like structures. The formation of the nanostructures can be clearly seen from the images with different magnifications in Figure 4.1 (d – f).

Longer time of deposition process has caused an increment in conductivity, resulting to the agglomeration of more electrons in the area of Ag nanoparticles, which tend the nanoparticles to stack together as layers and thus, creating the formation of flower like structures at controllable sizes. The Ag micro-flowers consists of contrasting related plates, which produced a hierarchy structure and resulting to the formation of interstitial sites in a large number after a certain time of deposition process (Y.-W. Lin & Tang, 2015). Table 4.1 presents the measurement of the height of Ag structures deposited and this measurement was used to build a model in simulations.

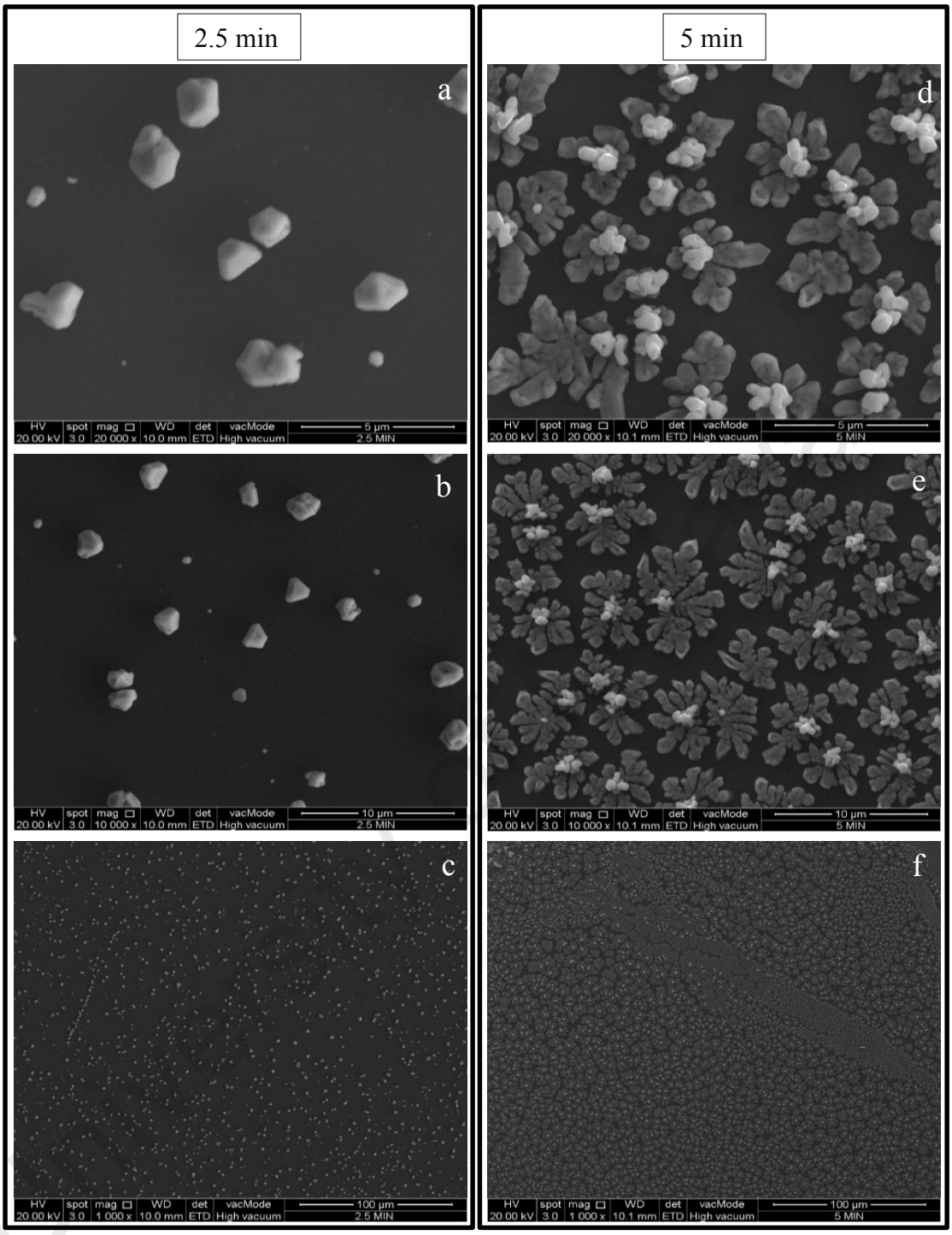

Figure 4.1: SEM image of Ag nanostructures with deposition time of 2.5 min at magnification of; a) ×20k, b) ×10k, c) ×1k, and deposition time of 5 min at magnification of; d) ×20k, e) ×10k, f) ×1k.

Table 4.1: Measurement of the height of Ag nanostructures deposited using surface profiler

Height of Ag nanoparticles from glass surfaces (nm)	Samples	
	2.5 min	**5.0 min**
1st reading	326.45	515.54
2nd reading	156.98	416.01
3rd reading	172.14	403.21
4th reading	216.12	443.44
5th reading	302.52	335.68
Average	**234.84**	**422.78**

4.2.2 CST Microwave Simulation software

In this simulation section, the shape and the thickness of Ag structures, shown in Figure 4.2 were drawn based on Figure 4.1 and measurement from the surface profiler (Table 4.1), respectively.

Figure 4.3 illustrates the e-field intensity distributions for the samples at 2.5 minutes and 5 minutes and these e-fields are highly distributed at 425 nm wavelength. The wavelength chooses to be at 425 nm as the highest intensity for this structures. The Ag structures were illuminated on a plane wave incident from *z* direction normal to the surface with the e-field being polarized in *y* direction. At 2.5 minutes, the e-field distributions show a low intensity of absorption due to the fewer Ag atoms were deposited, affecting a low LSPR effects, as shown in Figure 4.3(a). Contrastingly, a high e-field distributions of Ag structures occurred after 5 minutes of deposition time like in Figure 4.3(b) explains that the structures exhibited higher LSPR characteristics. Besides, based on SEM images in Figure 4.1 (d – f), the two particles of Ag microflower structures

were closed to each other which caused a smaller distance between those particles, thus, enhanced the local electrical field drastically.

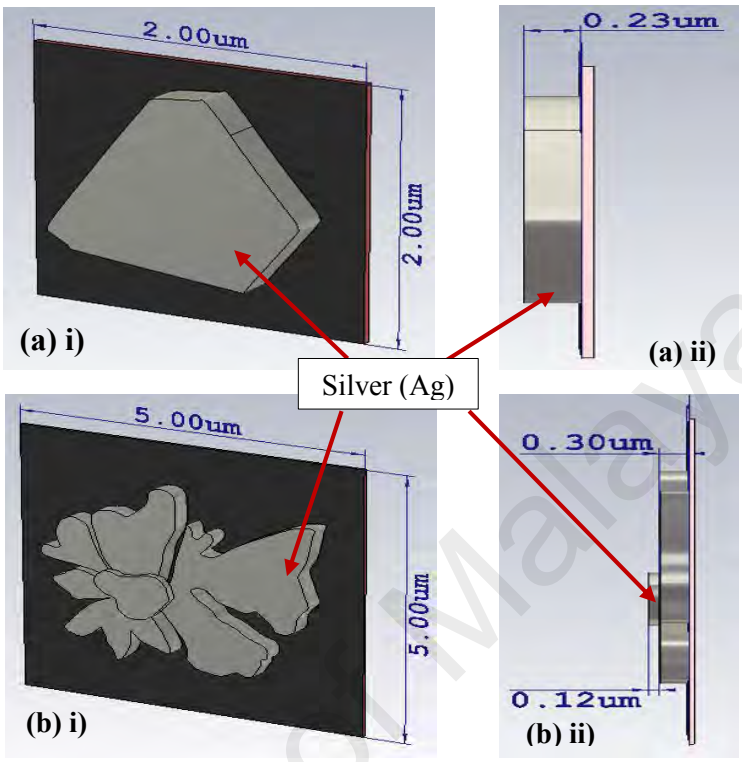

Figure 4.2: a) Ag structures at 2.5 min; i) front view, ii) side view, b)Ag structures at 5 min nanostructures; i) front view, ii) side view

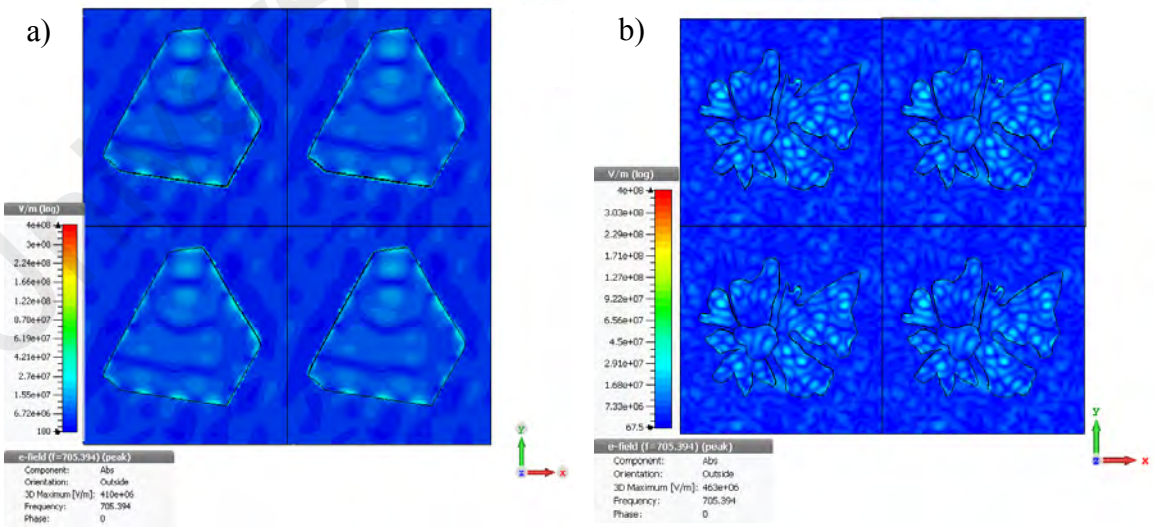

Figure 4.3: Electric field (e-field) intensity distributions under 425 nm incident wave for both samples at; a) 2.5 min, b) 5 min

Figure 4.4 shows the absorption spectrum obtained from the experimental data (a) and in comparison with the simulation (b), respectively. The diffusion of Ag particles happened because of the SPR absorption comes from the collective oscillations of electrons, caused by an electromagnetic (EM) field (Pandey et al., 2014). The UV-Vis absorption spectrum of the synthesized Ag structures at room temperature (from Figure 4.4 (a)) illustrated the maximum peak at 280 nm for both deposition times, but narrow peak are observed at 325 nm with obvious high absorbance intensity at 5 minutes. Meanwhile, Figure 4.4 (b) shows the absorption spectrum from the simulation, where the arrangement and spacing of the structures were constant. From the inset graph, the absorption peak displayed at 425 nm for 5 minutes while there is no obvious peak observed for the samples at 2.5 minutes; which the finding is contrasting with the experimental absorption spectrum.

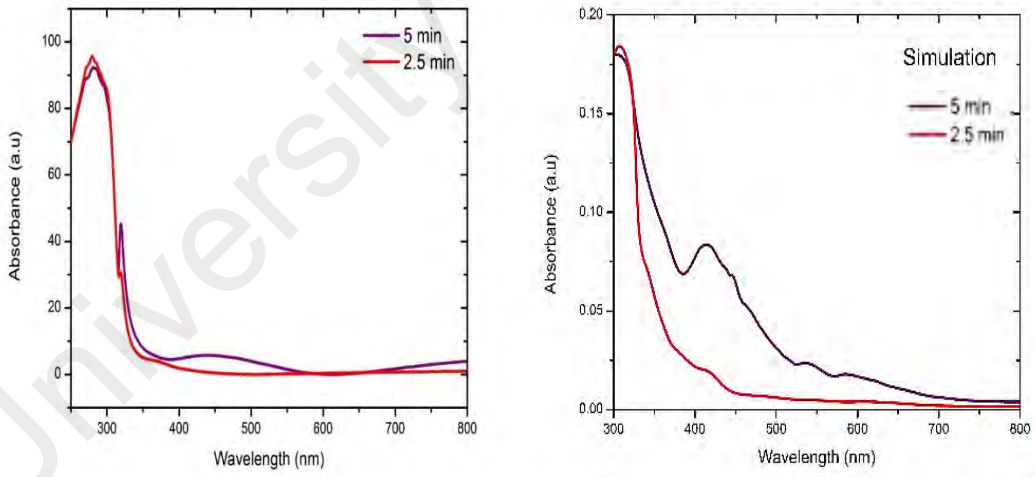

(a) (b)

Figure 4.4: (a) UV-Vis absorption spectra for Ag nanostructures from experimental, (b) simulated absorption spectrum; at 2.5 min and 5 min deposition times

4.3 Part B: Optical Characterization of AgNPs and TiO_2 Nanoparticles

4.3.1 Surface Morphology of AgNPs

Figure 4.5 shows the SEM images of Ag NPs deposited on the glass substrates with different thicknesses of 5 nm, 7 nm, 12 nm and 16 nm. The SEM analysis was employed to determine the size of the NPs and their distributions on the surface of the substrates. The annealing process take place at 170 °C for two hours demonstrates the Ag atoms started to accumulate to form Ag NPs from Ag in layer as it break down the surface energy on the substrate. From these images, it can be clearly seen that the particles tend to lose their spherical shape as the thickness of Ag films increases. Since Ag NPs were produced from thermal annealing process, the NPs are randomly distributed due to the surface tension and recrystallization process (Liu et al., 2015). However, at 5 nm thickness of Ag films, the formation and distributions of the NPs seems to be more uniform after annealing process. The average NPs size were obtained and showed in Table 4.3. From the table, apparently the size of Ag NPs increases with the increment of the film thickness.

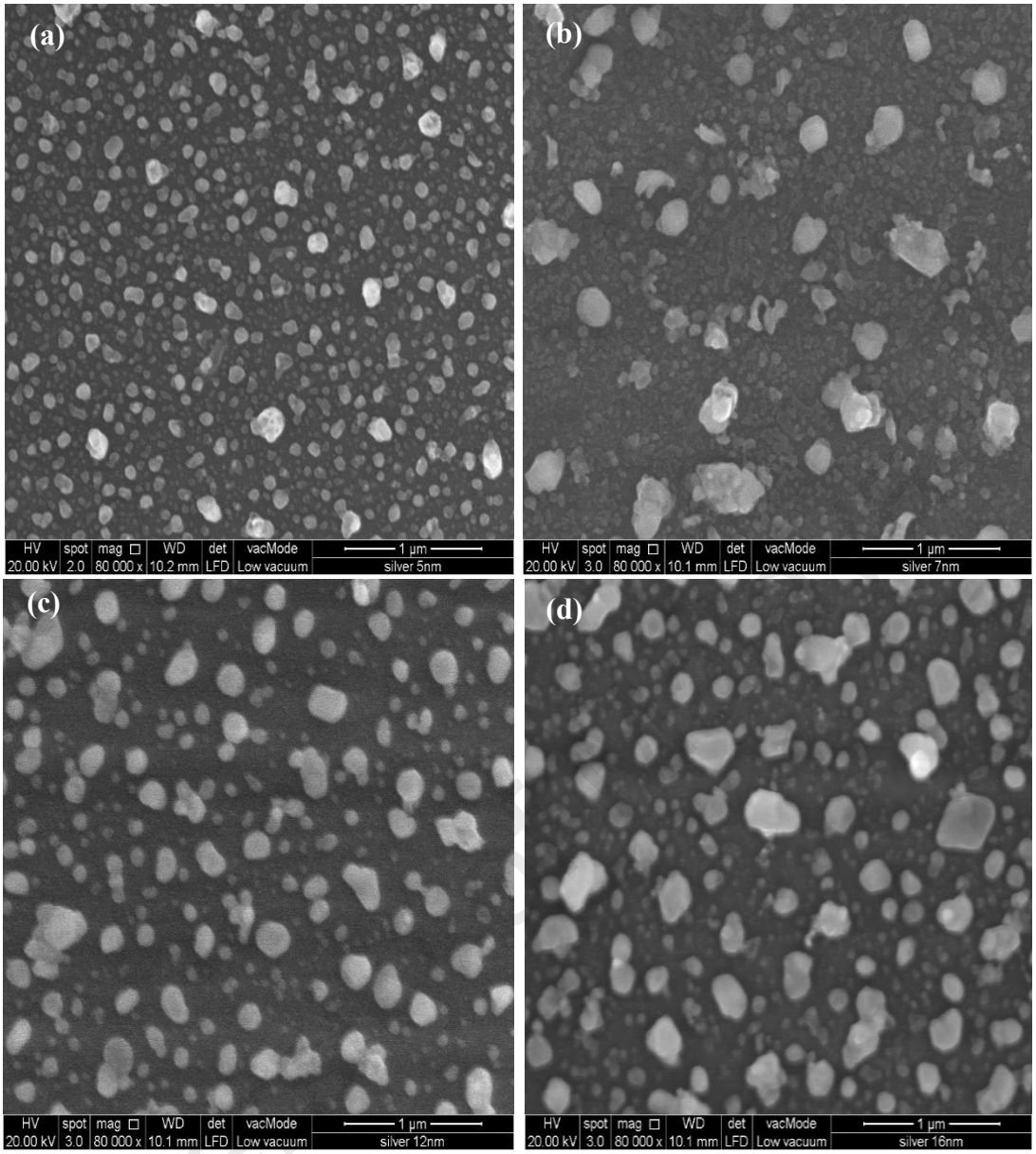

Figure 4.5: FESEM image of Ag NPs at different thickness at 80k x magnification; a) 5nm, b) 7nm, c) 12 nm, and d) 16 nm

Table 4.2: EDX analysis of all samples

Samples	Weight %		
	Si (Silicon)	**O (Oxygen)**	**Ag (Silver)**
5 nm	56.76	41.21	2.04
7 nm	31.23	45.76	2.31
12 nm	56.63	39.37	4.01
16 nm	53.9	40.16	5.94

Table 4.3: Average size of Ag nanoparticles at different thickness of Ag thin films

Thickness (nm)	Average size of Ag nanoparticles (nm)
5	40.11
7	54.43
12	90.86
16	102.68

4.3.2 Photoluminescence (PL) Measurement

PL spectra of AgNPs samples with four different thicknesses were displayed in Figure 4.6. In Figure 4.6 (a), a highest intensity dip was observed at 750 nm (1.6531 eV) along with other minor dip, located at 1100 nm (1.1271 eV). The wavelength is totally independent to the thickness of the metal films, but at the same time, the PL intensity decreases with the increase in thickness of the Ag thin films. After post annealing, bigger size of NPs were formed as the thickness of the deposited films was increased, which affects to the decrease in PL intensity. The reduction of PL intensity happened might be due to the decrease on the capacity of luminescent center. It is known that the annealing process can cause reduction of number of the surface states due to the increasing in the size of particles. The position and shape of peak and dip in PL intensity for all samples were stables, which caused by the equilibrium thermal temperature when annealing process to produce nanoparticles takes place.

Comparing the luminescence intensity of Ag/TiO_2 NPs in Figure 4.6 (b), it seems that the PL intensity was at the maximum when the thickest Ag thin film (16 nm) was covered with TiO_2. As observed in Figure 4.6b, a sharp peak were formed, centered at 1075 nm (1.1533 eV) and broader peak were formed at 560 nm (2.214 eV). The increase in PL intensity might be resulted from the relocation of charge between Ag molecules and conductance band of TiO_2. As AgNPs were having photoexcitation due to the plasmon effect, the formation of electron-hole pairs occurred which an excited electron from AgNPs was transferred to the conduction band of TiO_2 and simultaneously, a hole left by AgNPs is filled by a donor electron from the surrounding (S.-W. Lee, Obregon, & Rodriguez-Gonzalez, 2015). Incident photons are absorbed by TiO_2 particles with adequate energy that is equal or more than the band gap energy, however will produce photo induced charge carriers (R. Viter et al., 2012).

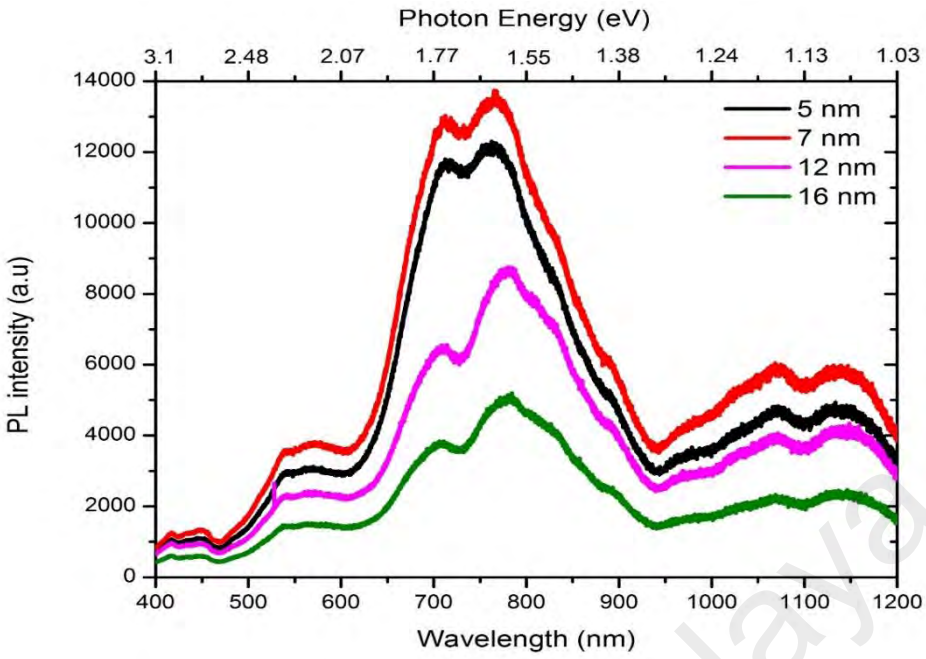

(a)

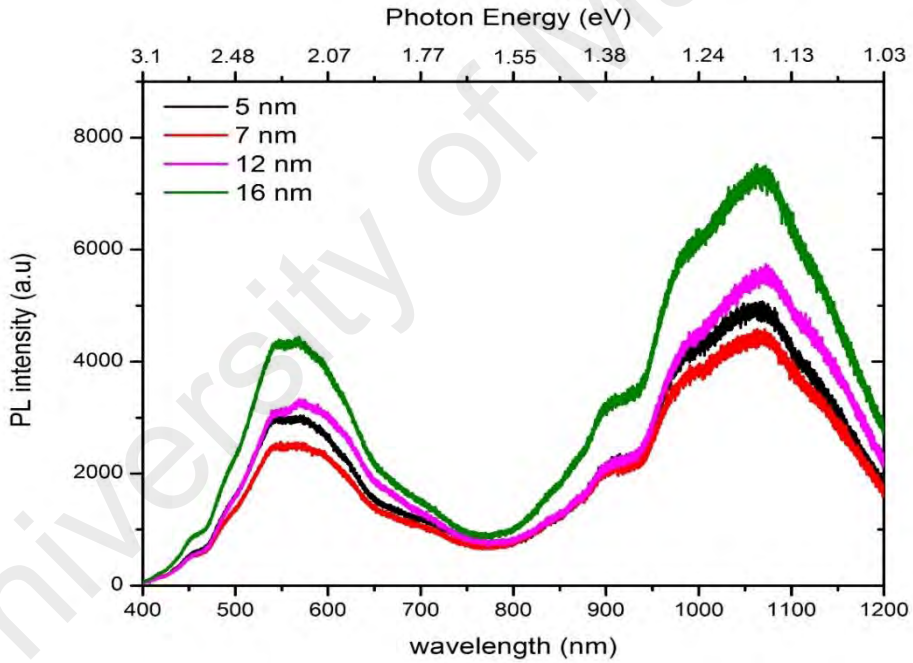

(b)

Figure 4.6: PL intensity of; (a) AgNPs, (b) Ag/TiO_2

4.3.3 UV-Vis Absorption Characterization

Figure 4.7 shows the absorption spectra of Ag NPs having different thicknesses of thin layer coating. Absorption band occurred when the frequency of incident photon (light) is at resonant with the collective oscillation of the electrons and known as SPR. In Figure 4.7(a), the SPR exhibit similar absorption behavior with peaks in a range between 280 nm and 300 nm, depending on the thickness of AgNPs layers.

Generally, the optical absorption behavior of metallic NPs is controlled by the SPR, which performs a red or blue shift in wavelength, totally depend on the size, shape, the aggregation and also surrounding by dielectric medium (Smitha, Nissamudeen, Philip, & Gopchandran, 2008). Practically, larger size of NPs likely to lose their spherical criteria as illustrated in Figure 4.5, causing the resonance wavelength to be slightly red shifted as a results of the changes in shape. Meanwhile, the intensity of the absorption band seems to be gradually increases as the thickness of the thin films increases. This shows the surface plasmon absorption intensity are depending upon the thickness of NPs layers, which gives effect to the shape and size of the NPs. The increment in absorption intensity happened due to the strong incident light being scattered or absorbed at the region of resonance wavelength of the particles as the size of the NPs increases (Pillai, Catchpole, Trupke, & Green, 2007). Besides, as the size of the NPs increase, the distances between the particles were decreased, arising a strong coupling effect between the particles.

Figure 4.7(b) illustrates the absorption spectra of Ag/TiO_2 with a thickness of 7 nm and 16 nm of Ag films under constant TiO_2 layer. The choice of thickness of Ag thin films were based on the performance of AgNPs in the PL measurements. Compared to the absorption spectra of the samples before deposition of TiO_2 layers, the resonance peaks are slightly shift to red-end. The red shift of the peaks are from 290 nm to 298 nm and from 295 nm to 300 nm for the samples of 7 nm and 16 nm, respectively. This shift

is referring to the increment of refractive index in the medium around the AgNPs. However, there are significant increments in absorption intensity when TiO_2 was deposited on the Ag layer. The increment in absorbance is the due to the improvement in photo excitation efficiency of TiO_2 (Tunc, Bruns, Gliemann, Grunze, & Koelsch, 2010).

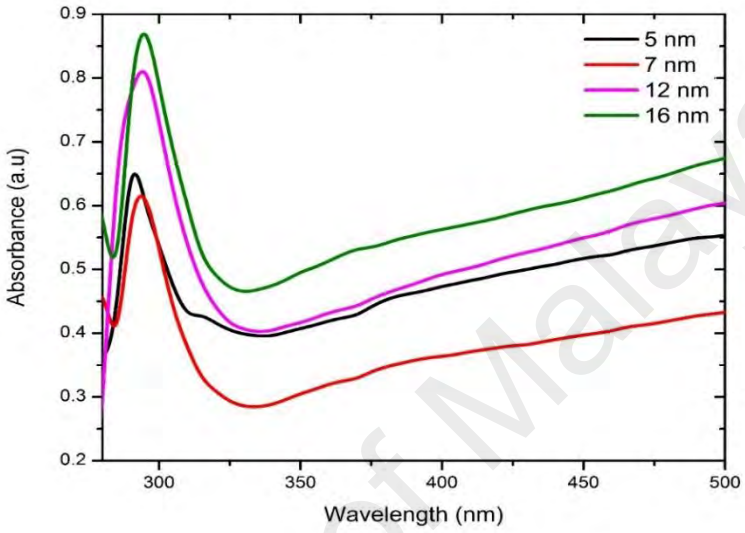

(a)

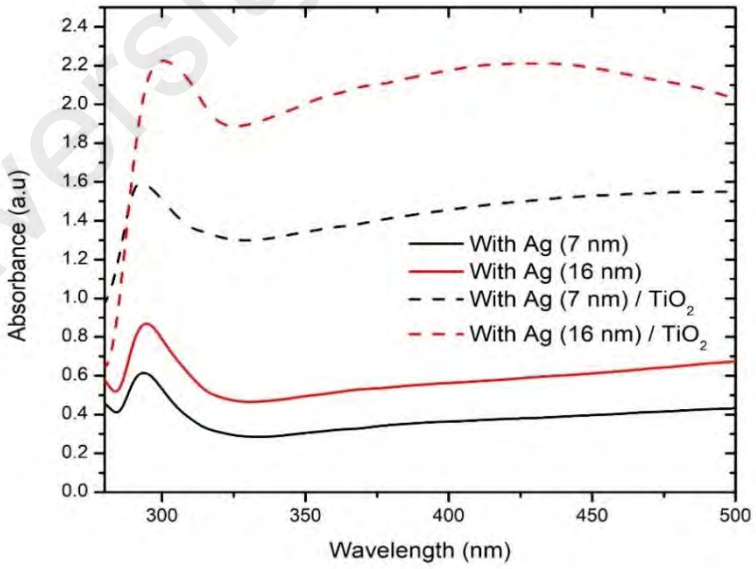

(b)

Figure 4.7: UV-Vis absorption spectra; (a) Different thickness of AgNPs, (b) AgNPs and Ag/TiO_2 with thickness of Ag layer at 7 nm and 16 nm

4.3.4 CST Microwave Studio Simulation for AgNPs

The shape of AgNPs are fixed to spherical shape but differed in sizes, as illustrated in Figure 4.8. The sizes of AgNPs were drawn based on the average measurement, obtained from Table 4.3. Figure 4.9 shows the intensity distribution of e-field for the samples at four thicknesses of Ag NPs thin layers. The e-field distribution of 7 nm Ag thin layer shows a high intensity and strong coupling effects between the particles, which results to higher LSPR effects on the particles. Contrastingly, a low absorption of e-field distribution in sample with 16 nm Ag thin layer shows that the NPs exhibit low LSPR characteristics. Although the size of particles for thickness of 16 nm Ag thin layer are bigger compared to others, the simulation shows that thickness of 7 nm Ag thin layer produced an optimum size of particles since e-field distribution displays a high intensity compared to others.

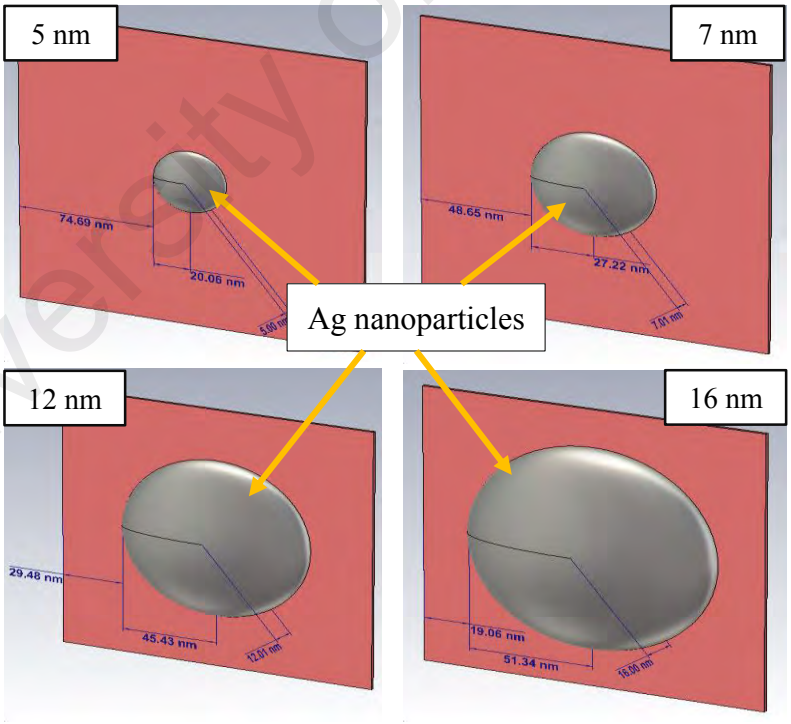

Figure 4.8: Different sizes of AgNPs drawn in CST simulation

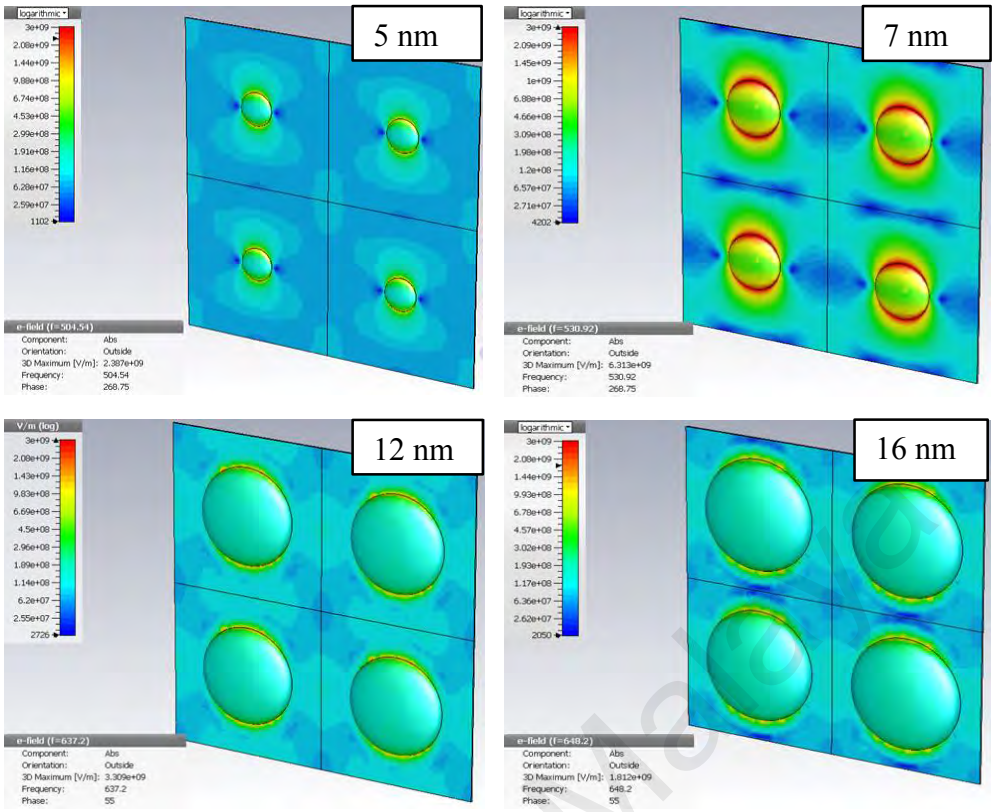

Figure 4.9: E-field intensity distributions for all the thicknesses of thin layer

4.4 Part C: Studies on Application of Optical Fiber as a Humidity Sensor

4.4.1 Sensing Mechanism of Optical Fiber Sensor

The operation principle of the optical fiber sensor is based on the interaction of the evanescent field with sensitive materials, specifically AgNPs and TiO_2 particles coated on the active region of the optical fiber. Since side polished optical fiber was used as sensing probe, an electromagnetic (EM) field that propagates inside the core of the fiber (known as guided wave) does not completely confined as half of the EM field was propagated outside the core of the optical fiber (known as evanescent wave). The guided wave will be affected if the evanescent field experienced any changes which in this case, the changes in surrounding humidity inside the chamber. When water molecules from the humidity are absorbed by the coated materials that has hydrophilic properties, the refractive index of the material will changed. This will altered the optical properties of

the materials, causing the characteristic of the guided light to change which in turn, modifies the transmitted output power together with the spectrum signals.

4.4.2 Experimental Results on Humidity Sensor

In this section, a single mode optical fiber with the size of 8.2 μm core diameter was polished to study the response of the fiber as a sensor in different relative humidity sensor. For comparison, the side polished optical fiber were coated with silver (Ag) at 7 nm and 16 nm thickness and covered with constant layer of TiO_2. AgNPs and TiO_2 particles were introduced as external layers in order to replace the cladding of the fiber in order to achieve best performance and good sensitivity of the sensor. This experiment was conducted in a controlled environment chamber with precise humidity control system.

Figure 4.10(a) illustrates the relative humidity with respect to resonance wavelength of the output spectrum. The graph shows that the initial resonance wavelength (at 50 %RH) shifted to larger value when the side polished fiber were coated with Ag at 7 nm and 16 nm, under constant TiO_2 layer. Initially, the wavelength is shifting from 1530.344 nm to 1531.768 nm (for Ag (7 nm)) and shifted to 1533.5754 nm after TiO_2 was dropped on the 7 nm of Ag layer. Meanwhile, after the fiber was coated with 16 nm of Ag layer, the wavelength are shifted to 1531.780 nm and then slightly shifted to 1531.985 nm for samples of Ag (16nm)/TiO_2. Further analysis of the resonance wavelength shifting is displayed in Figure 4.10(b). As the relative humidity values increases, the resonance wavelength shifted to blue shift (shorter wavelength). This shows that the sensing probes is sensitive and can response to any change in the environments, which in this case, the humidity of the surrounding area.

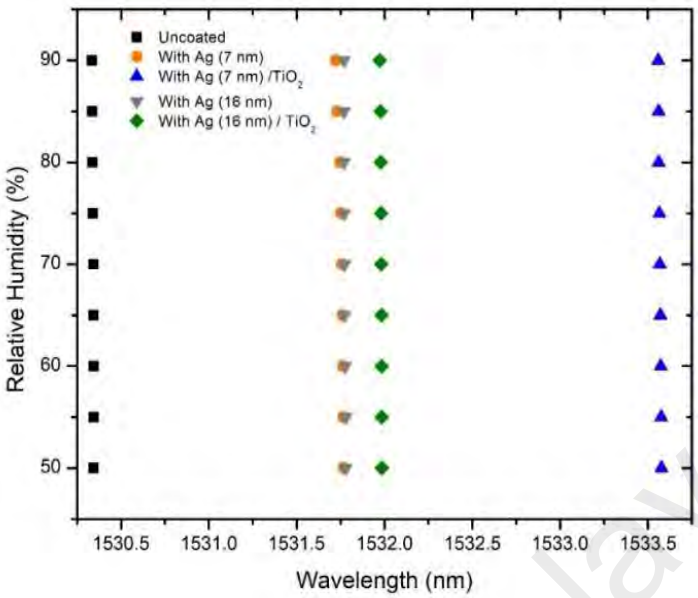

(a)

Figure 4.10: Comparison of relative humidity with respect to wavelength (a) Uncoated, Ag and Ag/TiO_2 at 7 nm and 16 nm thickness, (b) relative humidity with respected to wavelength for all samples

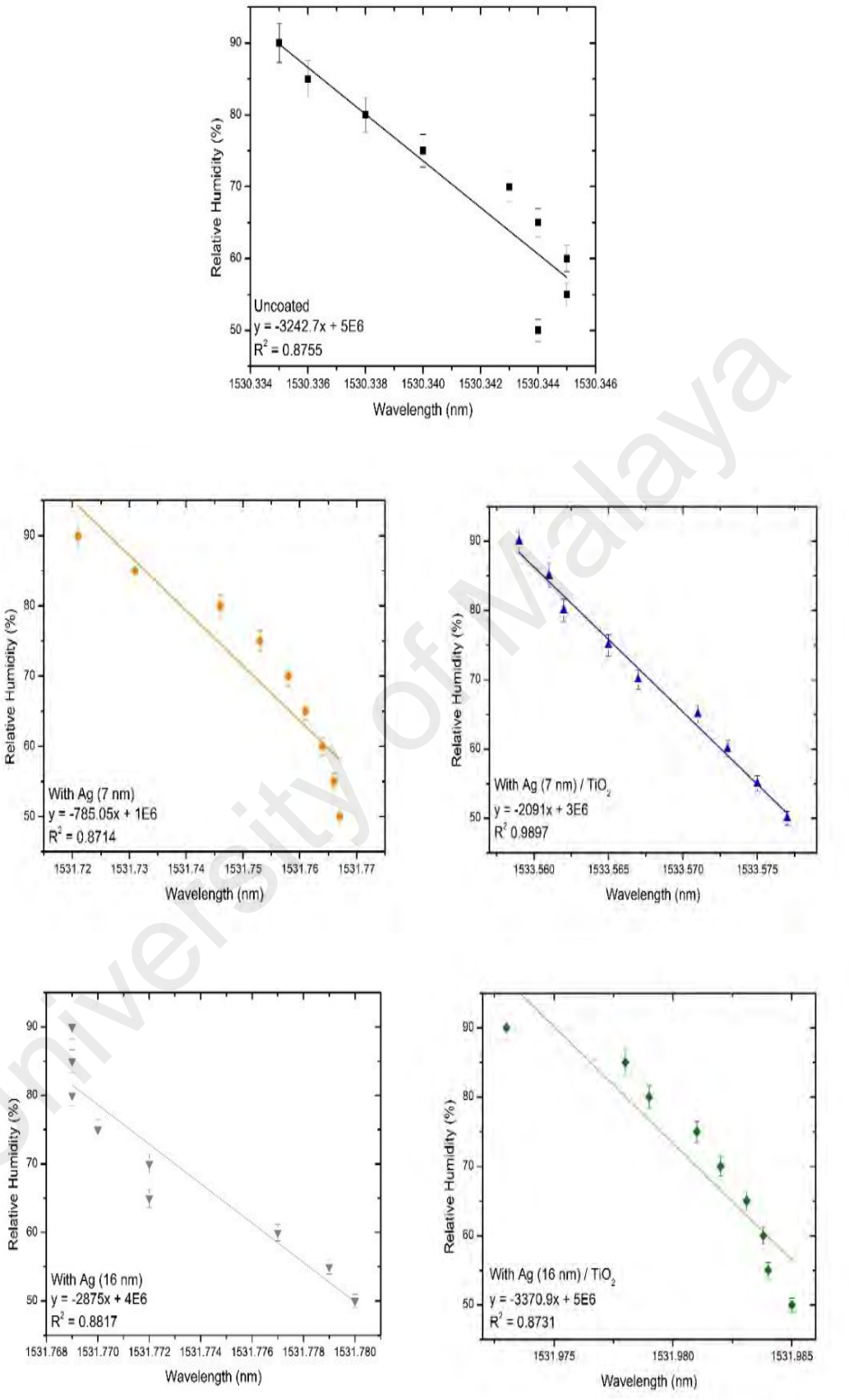

(b)

Figure 4.10, continued

Figure 4.11(a) shows the experimental results of transmittance output power with respect to relative humidity for uncoated side polished optical fiber with coated material sensors. The comparison shows increment in transmitted power when the fiber were coated with AgNPs and TiO_2 solution. When the polished region covered with AgNPs at 7 nm and 16 nm thickness, the initial output power seems to be increased by 2.82 mW and 1.5 mW at 50 %RH, respectively, indicating that Ag coating enhanced the humidity detector. As the relative humidity changes, the moisture from the surrounding was absorbed by the AgNPs which lead to the changes of the output power. Meanwhile, while adding another layer, which is TiO_2 solution on top of the AgNPs, an increment of power was at highest which is from 4.40 mW to 8.93 mW for Ag (7 nm) and from 3.08 mW to 8.05 mW for Ag (16 nm) at 50 %RH.

Since the changes in output power for each sample are small throughout the experiment, Figure 4.11(b) illustrates the transmitted output power with respect to relative humidity for each sample. As observed, the output power of sensor Ag (16 nm)/ TiO_2 seems to be decreased as the percentage of humidity increased. At higher relative humidity, the ions of water moisture were captured by the AgNPs, causing an increment in electron mobility in Ag films, thus, resulting the output power to be decreased (Chen & Lu, 2005)**.** Also, the lowering in output power can be explained by the change in density of composite layer after adsorption of water molecules. In terms of graph slope, the uncoated fiber shows small negative slope (-0.6933) compared to sensor of Ag (16 nm) (slope = -0.73) and sensor of Ag (16 nm)/ TiO_2 (slope = -1.2367), indicate that the sensor is less sensitive as the output power was decreased slowly when compared to relative humidity. Meanwhile, large negative slope produced by the sensor of Ag (16 nm)/ TiO_2 proved that the output power of the sensor decreased rapidly as the relative humidity increased constantly.

On the other hand, when the fiber was coated with Ag (7 nm) / TiO_2, the output power were increased as the humidity increased. This condition happened due to smaller particles size of AgNPs offer more active sites for water molecules interaction which will give a better sensitivity for the sensor. Based on the observation in Figure 4.11 (b), the sensor of Ag (7 nm) and sensor of Ag (7 nm) / TiO_2 shows positive slope which is contrasting with the results for the other three sensors. Small positive slope shows by sensor of Ag (7 nm) indicate that the output power of the sensor are slowly increased while the output power of sensor with Ag (7 nm) / TiO_2 coating were increased rapidly when the humidity inside the chamber increased constantly. Comparing the linear trend line for all sensors, the value of R^2 displayed by sensor of Ag (7 nm) / TiO_2 is the highest (0.9201), indicate that the line of the data produced is nicely fit in the graph. Meanwhile, the percentage of uncertainty in the measured data (in Figure 4.11 (b)) for each sensors are as follows; (Uncoated = ± 0.1 %, Ag (7 nm) = ± 0.2 %, Ag (7 nm)/ TiO_2 = ± 0.35 %, Ag (16 nm) = ± 0.05 %, and Ag (16 nm)/ TiO_2 = ± 0.05 %).

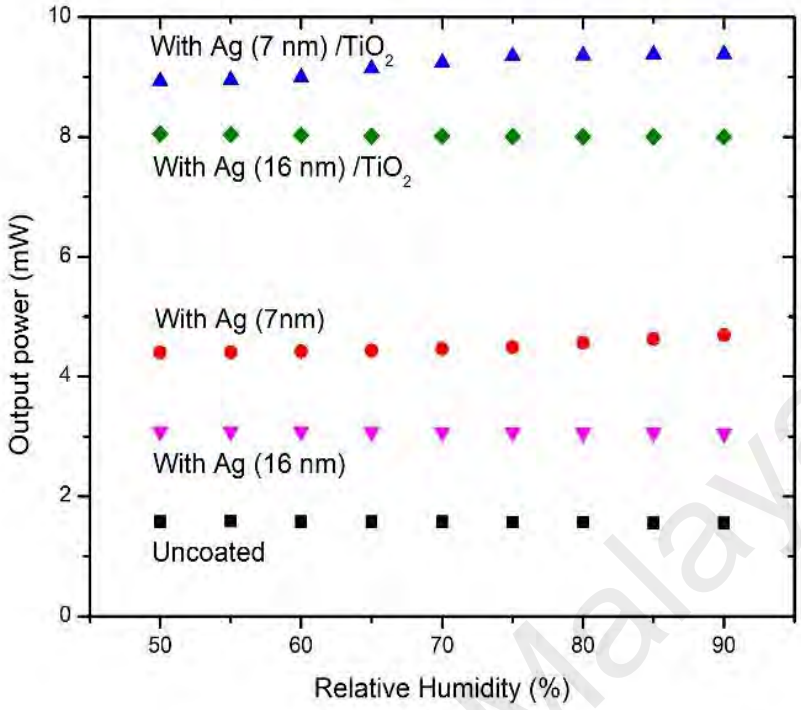

(a)

Figure 4.11: Comparison of transmitted output power with respect to relative humidity (a) Uncoated, TiO_2, Ag and Ag/TiO_2 at 7 nm and 16 nm thickness, (b) transmitted output power of all samples with respect to relative humidity

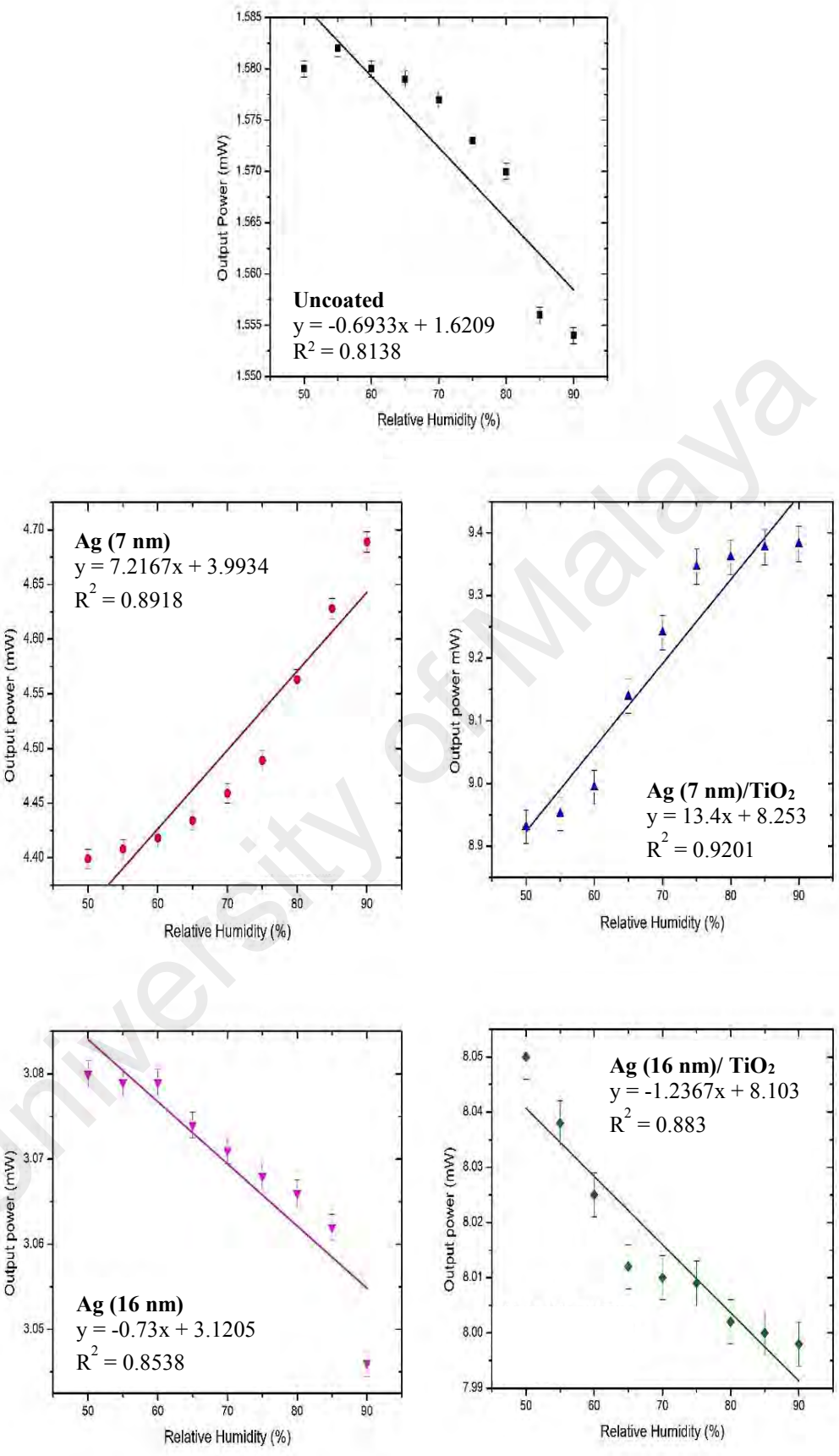

(b)

Figure 4.11, continued

Table 4.4 shows the performance of the side polished fiber coated with Ag and TiO_2 as a humidity sensor. The resolution of the sensor was obtained by dividing the standard deviation of the measurements with the sensitivity of the sensor. Meanwhile, the linearity was obtained from the correlation coefficient, R which is a measurement of the reliability of linear relationship between input and output parameters. The linearity of the sensor increases as the value of *R* approaching 100%. Based on Table 4.4, when the sensing probe was coated with the NPs, the sensitivity and linearity seems to be enhanced. This enhancement happened due to the effect of water moisture in the sensing layers. From the observation, sensor with Ag (7 nm) /TiO_2 coating shows the best performance as a humidity sensor since the probe exhibit good sensitivity and linearity at 92% and 13.4 mW/ %RH, respectively. Throughout the experiment, it was proved that the performance of the sensing probe is enhanced after being coated with those NPs.

Table 4.4: Performance of the side polished fiber as humidity sensor based on transmitted output power

Parameter	**Uncoated**	**Ag (7 nm)**	**Ag (7 nm) / TiO_2**	**Ag (16 nm)**	**Ag (16 nm) / TiO_2**
Standard Deviation (mW)	0.011	0.56	0.022	0.024	0.034
Resolution (%RH)	0.0158	0.0776	0.0016	0.329	0.0275
Linearity (%)	81.38	89.18	92.01	85.38	88.30
Sensitivity (mW/% RH)	0.6933	7.2167	13.400	0.7300	1.2367

CHAPTER 5: CONCLUSIONS

In this thesis, a few efforts are presented in producing silver nanoparticles with different structures to study their optical performance and their significance in enhancing the performance of plasmonics devices.

In the first part, the study includes both simulation and experimental approach. The silver flower likes and irregular edges structures (hexagonal) were deposited experimentally using electrochemical deposition technique. For the simulation studies, CST Microwave Studios was used to observe the performance of the silver nanoparticles in terms of electromagnetic fields. The simulation of 2D configurations using CST proved that the electromagnetic field was enhanced as the size of the structures are enlarged. This enhancement is due to the morphology of the flower-like structures, which provides larger areas and thus, resulting a high field enhancement factors.

Apart from that, the effect of varying thicknesses of silver nanoparticles film has also been studied. From the measurement based on SEM images, larger size of silver nanoparticles were formed as the thickness of the silver layer increased. At the same time, data obtained from PL measurements confirms that the absorption intensity is decreased when the thickness of silver layers increases due to the diminishing in luminescent center. Another sets of data from UV-Vis absorption measurement were done and shows that the absorption intensities are increased with the increasing in Ag layer thickness. A simulation work was done using CST Microwave Studio and it was observed that 7 nm thickness of Ag layer shows the highest distribution of E-field intensity compared to other samples of Ag nanoparticles. Another layer of metallic oxides, specifically titanium oxide (TiO_2) was introduced to cover the silver nanoparticles layer from oxidized. The presence of TiO_2 has shown a significant impact to the measurement of photoluminescence and UV-Vis absorption intensities.

The optimum thickness of silver layer preferred from the photoluminescence and absorption measurement was used to fabricate on side polished optical fiber as a humidity sensor. TiO_2 has proved that this metal oxides helped to increase and stabilized the performance of the sensing system. Although the changes in output measurement are relatively small, still this sensor are sensitive and can response to any changes in the environment. Based on the transmitted output power measurement, sensors of Ag (7 nm)/ TiO_2 coating shows a good performance as a humidity sensor with sensitivity and linearity of 92 % and 13.4 mW/%RH. Hence, integrating Ag and TiO_2 nanoparticles in sensor was considerable stable; however, it needs to have an improvement in the fabrication process for further development in sensing application.

5.1 Future Work

Our work has demonstrated two factors that altered the performance of LSPR characteristics, which are effects on varying shapes and thickness of silver nanostructures, and also the application of side polished optical fiber as humidity sensor which is simple in fabrication, affordable to be applied and easy to handle. First of all, other factors such as dielectric constant of the surrounding environment of the metallic thin layer, distance between nanoparticles and also the composition of medium used can be observed in order to see the changes in the performance of LSPR characteristics. Since silver structures have been used in this work, different noble metal such as gold, aluminum, and copper can be applied so that comparison between noble metal can be observed.

Furthermore, different noble metals can be introduced as a coating on the side polished optical fiber, to observe the performance of the sensor, especially the aspect of sensitivity. On top of, combination of different types of noble metal and metal oxides can be further investigated if any of these materials increased the efficiency of the sensor. Having a different polishing depth and length of the side polished optical fiber can be tailored since

this will affect the end performance of the sensor. Lastly, the performance of the sensor will also improve if the polished area of the fiber can be smoother and more uniform.

REFERENCES

Andersson, M., Österlund, L., Ljungström, S., & Palmqvist, A. (2002). Preparation of nanosize anatase and rutile TiO_2 by hydrothermal treatment of microemulsions and their activity for photocatalytic wet oxidation of phenol. *The Journal of Physical Chemistry B, 106*(41): 10674-10679.

Aneesh, R., & Khijwania, S. K. (2012). Titanium dioxide nanoparticle based optical fiber humidity sensor with linear response and enhanced sensitivity. *Applied Optics, 51*(12): 2164-2171.

Aris, A. M., Rahman, H. A., Irawati, N., Harun, S. W., Lim, K.-S., & Ahad, I. Z. M. (2017). Enhanced Relative Humidity Sensing Based on a Tapered Fiber Bragg Grating with Zinc Oxide Nanostructure-Embedded Coatings. *Advanced Science Letters, 23*(6): 5452-5456.

Bariáin, C., Matías, I. R., Arregui, F. J., & López-Amo, M. (2000). Optical fiber humidity sensor based on a tapered fiber coated with agarose gel. *Sensors and Actuators B: Chemical, 69*(1): 127-131.

Bessekhouad, Y., Robert, D., & Weber, J. (2003). Preparation of TiO_2 nanoparticles by sol-gel route. *International Journal of Photoenergy, 5*(3): 153-158.

Boken, J., Khurana, P., Thatai, S., Kumar, D., & Prasad, S. (2017). Plasmonic nanoparticles and their analytical applications: A review. *Applied Spectroscopy Reviews*, *52*(9): 774-820.

Cai, W., & Shalaev, V. M. (2010). *Optical metamaterials* (Vol. 10): Springer.

Caucheteur, C., Guo, T., & Albert, J. (2015). Review of plasmonic fiber optic biochemical sensors: improving the limit of detection. *Analytical and bioanalytical chemistry, 407*(14): 3883-3897.

Chen, Z., & Lu, C. (2005). Humidity sensors: a review of materials and mechanisms. *Sensor letters, 3*(4): 274-295.

Chiu, M.-H., Shih, C.-H., & Chi, M.-H. (2007). Optimum sensitivity of single-mode D-type optical fiber sensor in the intensity measurement. *Sensors and Actuators B: Chemical, 123*(2): 1120-1124.

Clohessy, A. M., Healy, N., Murphy, D. F., & Hussey, C. D. (2005). Short low-loss nanowire tapers on singlemode fibres. *Electronics Letters, 41*(17): 954-955.

Daubinger, P., Kieninger, J., Unmussig, T., & Urban, G. A. (2014). Electrochemical characteristics of nanostructured platinum electrodes - a cyclic voltammetry study. *Physical Chemistry Chemical Physics, 16*(18): 8392-8399.

De-Jun, F., Mao-Sen, Z., Liu, G., Xi-Lu, L., & Dong-Fang, J. (2014). D-shaped plastic optical fiber sensor for testing refractive index. *IEEE Sensors Journal, 14*(5): 1673-1676.

Fernando, R., Semendy, F., & Wijewarnasuriya, P. (2012). *Altering Plasmonic Nanoparticle Size Through Thermal Annealing for Improved Photovoltaic Devices*. Army Research Lab Adelphi Md Sensors And Electron Devices Directorate.

Freise, A. (2012). Optical Metamaterials: Fundamentals and Applications, by W. Cai and V. Shalaev. *Contemporary Physics, 53*(3): 278-279.

Grazia, A., Riccardo, M., & Ciaccheri, F. L. (1998). Evanescent wave absorption spectroscopy by means of bi-tapered multimode optical fibers. *Applied Spectroscopy, 52*(4): 546-551.

Gupta, B. D., & Verma, R. K. (2009). Surface plasmon resonance-based fiber optic sensors: principle, probe designs, and some applications. *Journal of Sensors, 2009*: 12.

Gupta, G., & Kondoh, J. (2007). Tuning and sensitivity enhancement of surface plasmon resonance sensor. *Sensors and Actuators B: Chemical, 122*(2): 381-388.

Hamdan, K. S., Abdullah, S. M., Sulaiman, K., & Zakaria, R. (2014). Effects of silver nanoparticles towards the efficiency of organic solar cells. *Applied Physics A, 115*(1): 63-68.

Harun, S., Lim, K., Tio, C., Dimyati, K., & Ahmad, H. (2013). Theoretical analysis and fabrication of tapered fiber. *Optik-International Journal for Light and Electron Optics, 124*(6): 538-543.

Hong, Y., Huh, Y.-M., Yoon, D. S., & Yang, J. (2012). Nanobiosensors based on localized surface plasmon resonance for biomarker detection. *Journal of Nanomaterials, 2012*: 111.

Hou, Y.-Q., Zhuang, D.-M., Zhang, G., Zhao, M., & Wu, M.-S. (2003). Influence of annealing temperature on the properties of titanium oxide thin film. *Applied Surface Science, 218*(1): 98-106.

Huang, Y., Zhu, W., Li, Z., Chen, G., Chen, L., Zhou, J., . . . Yu, J. (2018). High-performance fibre-optic humidity sensor based on a side-polished fibre wavelength selectively coupled with graphene oxide film. *Sensors and Actuators B: Chemical, 255*: 57-69.

Iga, M., Seki, A., & Watanabe, K. (2004). Hetero-core structured fiber optic surface plasmon resonance sensor with silver film. *Sensors and Actuators B: Chemical, 101*(3): 368-372.

Jha, R., Verma, R. K., & Gupta, B. (2008). Surface plasmon resonance-based tapered fiber optic sensor: sensitivity enhancement by introducing a Teflon layer between core and metal layer. *Plasmonics, 3*(4): 151.

Kinnan, M. K., & Chumanov, G. (2010). Plasmon coupling in two-dimensional arrays of silver nanoparticles: II. Effect of the particle size and interparticle distance. *The Journal of Physical Chemistry C, 114*(16): 7496-7501.

Kittel, C. (2005). *Introduction to solid state physics*: Wiley.

Klantsataya, E., François, A., Ebendorff-Heidepriem, H., Hoffmann, P., & Monro, T. M. (2015). Surface plasmon scattering in exposed core optical fiber for enhanced resolution refractive index sensing. *Sensors, 15*(10): 25090-25102.

Knight, M. W., King, N. S., Liu, L., Everitt, H. O., Nordlander, P., & Halas, N. J. (2014). Aluminum for Plasmonics. *ACS nano, 8*(1): 834-840.

Kroo, N., Szentirmay, Z., & Walther, H. (2005). Sub-wavelength microscopy of surface plasmon oscillations and their statistical properties. *Surface Science, 582*(1): 110-116.

Kude, V. P., & Khairnar, R. (2008). Fabrication and numerical evaluation of the tapered single mode optical fiber: Detection of change in refractive index.

Lee, K.-S., & El-Sayed, M. A. (2006). Gold and silver nanoparticles in sensing and imaging: sensitivity of plasmon response to size, shape, and metal composition. *The Journal of Physical Chemistry B, 110*(39): 19220-19225.

Lee, S.-W., Obregon, S., & Rodriguez-Gonzalez, V. (2015). The role of silver nanoparticles functionalized on TiO_2 for photocatalytic disinfection of harmful algae. *RSC Advances, 5*(55): 44470-44475.

Li, X., Hong, Z., & Sun, X. (2011). Photonic nano-device for optical signal processing. *Frontiers of Optoelectronics in China, 4*(3): 254.

Liao, C., Wang, Q., Xu, L., Liu, S., He, J., Zhao, J., . . . Wang, Y. (2016). D-shaped fiber grating refractive index sensor induced by an ultrashort pulse laser. *Applied Optics, 55*(7): 1525-1529.

Lin, H.-Y., Huang, C.-H., Cheng, G.-L., Chen, N.-K., & Chui, H.-C. (2012). Tapered optical fiber sensor based on localized surface plasmon resonance. *Optics Express, 20*(19): 21693-21701.

Lin, Y.-W., & Tang, C. (2015). Electrochemical synthesis and deposition of surface-enhanced Raman scattering-active silver microstructures on a screen-printed carbon electrode. *The Journal of Physical Chemistry C, 119*(44): 24865-24874.

Liu, X., Li, D., Sun, X., Li, Z., Song, H., Jiang, H., & Chen, Y. (2015). Tunable Dipole Surface Plasmon Resonances of Silver Nanoparticles by Cladding Dielectric Layers. *Scientific reports, 5*: 12555.

Malekshahi Byranvand, M., Nemati Kharat, A., Fatholahi, L., & Malekshahi Beiranvand, Z. (2013). A review on synthesis of nano-TiO_2 via different methods. *Journal of nanostructures, 3*(1): 1-9.

Martinsson, E. (2014). *Nanoplasmonic Sensing Using Metal Nanoparticles*. Linköping University Electronic Press.

Mendes, P. M., Jacke, S., Critchley, K., Plaza, J., Chen, Y., Nikitin, K., . . . Fitzmaurice, D. (2004). Gold Nanoparticle Patterning of Silicon Wafers Using Chemical e-Beam Lithography. *Langmuir, 20*(9): 3766-3768.

Mie, G. (1908). Beiträge zur Optik trüber Medien, speziell kolloidaler Metallösungen. *Annalen der physik, 330*(3): 377-445.

Mishra, S. K., Bhardwaj, S., & Gupta, B. D. (2015). Surface plasmon resonance-based fiber optic sensor for the detection of low concentrations of ammonia gas. *IEEE Sensors Journal, 15*(2): 1235-1239.

Mitsushio, M., Miyashita, K., & Higo, M. (2006). Sensor properties and surface characterization of the metal-deposited SPR optical fiber sensors with Au, Ag, Cu, and Al. *Sensors and Actuators A: Physical, 125*(2): 296-303.

Morales, A. M., & Lieber, C. M. (1998). A Laser Ablation Method for the Synthesis of Crystalline Semiconductor Nanowires. *Science, 279*(5348): 208-211.

Murray, W. A., & Barnes, W. L. (2007). Plasmonic materials. *Advanced Materials, 19*(22): 3771-3782.

Nehl, C. L., Liao, H., & Hafner, J. H. (2006). Optical properties of star-shaped gold nanoparticles. *Nano letters, 6*(4): 683-688.

Nguyen, H. H., Park, J., Kang, S., & Kim, M. (2015). Surface plasmon resonance: a versatile technique for biosensor applications. *Sensors, 15*(5): 10481-10510.

Ouyang, T., Lin, L., Xia, K., Jiang, M., Lang, Y., Guan, H., . . . Chen, Z. (2017). Enhanced optical sensitivity of molybdenum diselenide ($MoSe_2$) coated side polished fiber for humidity sensing. *Optics Express, 25*(9): 9823-9833.

Pandey, J. K., Swarnkar, R., Soumya, K., Dwivedi, P., Singh, M. K., Sundaram, S., & Gopal, R. (2014). Silver nanoparticles synthesized by pulsed laser ablation: as a potent antibacterial agent for human enteropathogenic gram-positive and gram-negative bacterial strains. *Appl Biochem Biotechnol, 174*(3): 1021-1031.

Pavaskar, P., Theiss, J., & Cronin, S. B. (2012). Plasmonic hot spots: nanogap enhancement vs. focusing effects from surrounding nanoparticles. *Optics Express, 20*(13): 14656-14662.

Pillai, S., Catchpole, K., Trupke, T., & Green, M. (2007). Surface plasmon enhanced silicon solar cells. *Journal of applied physics, 101*(9): 093105.

Ramakrishna, G., & Ghosh, H. N. (2003). Optical and photochemical properties of sodium dodecylbenzenesulfonate (DBS)-capped TiO_2 nanoparticles dispersed in nonaqueous solvents. *Langmuir, 19*(3): 505-508.

Scuderi, M., Esposito, M., Todisco, F., Simeone, D., Tarantini, I., De Marco, L., . . . Cuscunà, M. (2016). Nanoscale Study of the Tarnishing Process in Electron Beam Lithography-Fabricated Silver Nanoparticles for Plasmonic Applications. *The Journal of Physical Chemistry C, 120*(42): 24314-24323.

Sharma, A. K., Jha, R., & Gupta, B. (2007). Fiber-optic sensors based on surface plasmon resonance: a comprehensive review. *IEEE Sensors Journal, 7*(8): 1118-1129.

Shukla, S., Bharadvaja, A., Parashar, G., Mishra, A., Dubey, G., & Tiwari, A. (2012). Fabrication of ultra-sensitive optical fiber based humidity sensor using TiO_2 thin film. *Adv. Mater. Lett, 3*: 365-370.

Smitha, S., Nissamudeen, K., Philip, D., & Gopchandran, K. (2008). Studies on surface plasmon resonance and photoluminescence of silver nanoparticles. *Spectrochimica Acta Part A: Molecular and Biomolecular Spectroscopy, 71*(1): 186-190.

Srivastava, S. K., & Gupta, B. D. (2013). Fiber optic plasmonic sensors: past, present and future. *The Open Optics Journal, 7*(1): 58-83.

Takagi, K., Sasaki, H., Seki, A., & Watanabe, K. (2010). Surface plasmon resonances of a curved hetero-core optical fiber sensor. *Sensors and Actuators A: Physical, 161*(1): 1-5.

Thi My Dung, D., Thi Tuyet Thu, L., Eric, F.-B., & Mau Chien, D. (2011). Synthesis and optical properties of copper nanoparticles prepared by a chemical reduction method. *Advances in Natural Sciences: Nanoscience and Nanotechnology, 2*(1): 015009.

Tian, M., Lu, P., Chen, L., Lv, C., & Liu, D. (2012). All-solid D-shaped photonic fiber sensor based on surface plasmon resonance. *Optics Communications, 285*(6): 1550-1554.

Tunc, I., Bruns, M., Gliemann, H., Grunze, M., & Koelsch, P. (2010). Bandgap determination and charge separation in Ag@ TiO_2 core shell nanoparticle films. *Surface and Interface Analysis, 42*(6-7): 835-841.

Urrutia, A., Goicoechea, J., & Arregui, F. J. (2015). Optical Fiber Sensors Based on Nanoparticle-Embedded Coatings. *Journal of Sensors, 2015*: 18.

Viter, R., Smyntyna, V., Starodub, N., A.Tereshchenko, Kusevitch, A., Doychoa, I., . . . Spigulis, J. (2012). Novel Immune TiO_2 Photoluminescence Biosensors for Leucosis Detection. *Procedia Engineering, 47*: 338-341.

Viter, R., Starodub, N., Smyntyna, V., Tereschenko, A., Kusevitch, A., Sitnik, J., . . . Macak, J. (2011). Immune biosensor based on silica nanotube hydrogels for rapid

biochemical diagnostics of bovine retroviral leukemia. *Procedia Engineering, 25*: 948-951.

Wahi, R. K., Liu, Y., Falkner, J. C., & Colvin, V. L. (2006). Solvothermal synthesis and characterization of anatase TiO_2 nanocrystals with ultrahigh surface area. *Journal of colloid and interface science, 302*(2): 530-536.

Wang, Q., Song, F., Lin, S., Liu, J., Zhao, H., Zhang, C., . . . Pun, E. Y. (2011). Optical properties of silver nanoprisms and their influences on fluorescence of europium complex. *Optics Express, 19*(8): 6999-7006.

Wang, X., Tian, K., Yuan, L., Lewis, E., Farrell, G., & Wang, P. (2018). A High-Temperature Humidity Sensor Based on a Singlemode-Side Polished Multimode-Singlemode Fiber Structure. *Journal of Lightwave Technology, 36*(13): 2730-2736.

Wang, Z., Shi, L., Wu, F., Yuan, S., Zhao, Y., & Zhang, M. (2011). The sol–gel template synthesis of porous TiO_2 for a high performance humidity sensor. *Nanotechnology, 22*(27): 275502.

Wood, R. W. (1902). On a remarkable case of uneven distribution of light in a diffraction grating spectrum. *Proceedings of the Physical Society of London, 18*(1): 269.

Xu, S., Man, B., Jiang, S., Wang, J., Wei, J., Xu, S., . . . Qiu, H. (2015). Graphene/Cu Nanoparticle Hybrids Fabricated by Chemical Vapor Deposition As Surface-Enhanced Raman Scattering Substrate for Label-Free Detection of Adenosine. *ACS applied materials & interfaces, 7*(20): 10977-10987.

Xu, W., Shi, J., Yang, X., Xu, D., Rong, F., Zhao, J., & Yao, J. (2017). Relative Humidity Sensor Based on No-Core Fiber Coated by Agarose-Gel Film. *Sensors, 17*(10): 2353.

Yockell-Lelièvre, H., Lussier, F., & Masson, J.-F. (2015). Influence of the particle shape and density of self-assembled gold nanoparticle sensors on lspr and sers. *The Journal of Physical Chemistry C, 119*(51): 28577-28585.

Zakaria, R., Yusoff, S. F. A. Z., Law, K. C., Lim, C. S., & Ahmad, H. (2017). Investigation on the Effects of the Formation of a Silver "Flower-Like Structure" on Graphene. *Nanoscale Research Letters, 12*(1): 50.

Zhang, J. Z., & Noguez, C. (2008). Plasmonic optical properties and applications of metal nanostructures. *Plasmonics, 3*(4): 127-150.

Zhang, Y., Gu, C., Schwartzberg, A., & Zhang, J. (2005). Surface-enhanced Raman scattering sensor based on D-shaped fiber. *Applied Physics Letters, 87*(12): 123105.

LIST OF PUBLICATIONS AND PAPER PRESENTED

Research Articles

Yusoff, S. F. A. Z., Lim, C. S., Azzuhri, S. R., Ahmad, H., & Zakaria, R. (2018). Studies of Ag/TiO_2 plasmonics structures integrated in side polished optical fiber used as humidity sensor. *Results in Physics*, 10, 308-316.

S. F. A. Z. Yusoff, M. H. Mezher, I. S. Amiri, N. Ayyanar, D. Vigneswaran, H. Ahmad, R. Zakaria (2018) Detection Of Moisture Content In Transformer Oil Using Platinum Coated On D-shaped Optical Fiber. *Optical Fiber Technology,* accepted on 2nd July 2018.

Zakaria, R., Yusoff, S. F. A. Z., Law, K. C., Lim, C. S., & Ahmad, H. (2017). Investigation on the Effects of the Formation of a Silver "Flower-Like Structure" on Graphene. *Nanoscale Research Letters, 12*(1), 50.

Zakaria, R., Kam, W., Ong, Y., Yusoff, S., Ahmad, H., & Mohammed, W. S. (2017). Fabrication and simulation studies on D-shaped optical fiber sensor via surface plasmon resonance. *Journal of Modern Optics*, 1-7.

Conferences

Energy, Material & Nanotechnology (**EMN**) Meeting on Light Matter Interactions, May 10 – 13, 2016, Singapore.

Photonics & Conference Meeting (**PCM**) 2016, August 15 – 16, 2016, University of Malaya, Kuala Lumpur, Malaysia.